IFRC | Global Disaster Preparedness Center

RESEARCH PAPER

Trees4HeatResilience:

Evaluating Tree Canopy Coverage to Reduce Air Conditioning Demand in Honduran Urban Neighborhoods

Juan Gamero-Salinas, *University of Navarra*
Mabel Morales-Otero, *University of Navarra*

2025

www.preparecenter.org

Table of Contents

Abstract

This research examines the neighborhood-level relationship between urban tree canopy coverage and air conditioning (A/C) usage in San Pedro Sula, Honduras, a rapidly growing city with high heat exposure. A computer vision model was retrained on local aerial imagery to segment tree canopies, which were combined with building footprints from OpenStreetMap (OSM) to calculate a neighborhood-level *tree-to-building ratio*. These data were integrated with census information on A/C usage and socioeconomic indicators (e.g., households with no unsatisfied basic needs, roof type). Results show that while overall *tree coverage* in the city is about 45%, canopy distribution is highly uneven. A/C usage shows a similar disparity, with 26.1% of households reporting at least one unit. Spatial regression analyses (e.g., Spatial Durbin Model, Leroux binomial model) reveal a strong inverse relationship between the *tree-to-building ratio* and A/C usage: doubling or tripling the ratio is associated with a 21–45% reduction in A/C usage. Also, the *tree-to-building ratio* proved a more reliable indicator of cooling benefits than overall *tree coverage*, which tends to align with wealthier areas that still display high A/C usage. These findings highlight the need for targeted greening in heat-exposed neighborhoods, supporting nature-based solutions for climate resilience in low-income tropical cities.

Keywords: trees, tree coverage, tree canopy, air conditioning, cooling, heat resilience, overheating

This work was part of a multi-country research initiative led by the Global Disaster Preparedness Center of the American Red Cross.

1. Introduction

Urban areas are at the forefront of the fight for climate resilience, with rising temperatures hitting cities the hardest. In tropical regions like Honduras, a lower middle-income country, cities are particularly vulnerable to heat stress induced by rapid urbanization rates that reduces green spaces and intensifies the urban heat island effect (UHI) (Angel et al., 2004; Carías, 2013; Mejía, 2018). The UHI effect occurs when built-up areas experience significantly higher temperatures than surrounding rural areas due to the concentration of heat-absorbing surfaces, like asphalt and concrete, coupled with a lack of vegetation and additional heat released from human activities (i.e. anthropogenic heat), such as vehicles, industry, and buildings. High-income countries typically benefit from greater natural vegetation coverage, such as forests and parks (Onishi et al., 2010), whereas surface UHI effects tend to intensify more rapidly in lower-income countries (Yuan et al., 2025). Consequently, urban overheating is a particularly urgent challenge in low-income cities, where tree canopy coverage is often limited. Indoor overheating in buildings, particularly those with air conditioning (A/C), is another concern. Recent studies indicate that homes equipped with A/C systems are often more susceptible to indoor overheating when the systems are turned off (J. C. Gamero-Salinas, Monge-Barrio, & Sánchez-Ostiz, 2020; J. C. Gamero-Salinas, Monge-Barrio, & Sanchez-Ostiz, 2020). This vulnerability arises because these buildings tend to rely heavily on mechanical cooling and often lack passive strategies such as effective natural ventilation (J. Gamero-Salinas et al., 2021; J. Gamero-Salinas & López-Fidalgo, 2024) or nature-based solutions like on-site trees that lower the UHI (Morakinyo et al., 2017). As a result, they exhibit lower thermal resilience in the face of rising outdoor temperatures.

1.1 Literature Review

Urban trees influence indoor cooling demand primarily through shading and evapotranspiration, which lower heat gains on building envelopes and mitigate the UHI effect in cities. Over the past decades, research has advanced from simulation-based analyses to controlled experiments and large-scale urban forestry programs. This literature review provides evidence that strategic integration of trees into urban design can reduce cooling energy use in buildings.

Simulation-Based Studies. A considerable portion of the literature employs energy simulation approaches to evaluate the cooling benefits of trees. A study (McPherson & Simpson, 2003) combined aerial canopy cover data with building energy models to estimate the energy savings of urban trees in 21 California cities. It found that the state's approximately 177.3 million existing trees reduce annual air conditioning energy use by 2.5%, **reflecting a modest but significant statewide average across diverse climates and**

building types. Additionally, these trees lower peak electricity demand by 10%, saving utilities an estimated $778.5 million annually, or roughly $4.39 per tree. In another study the same first author (McPherson & Rowntree, 1993) also found through monitoring and energy simulation studies that trees can be a cost-effective energy conservation measure for some electric utilities, with simulations suggesting that a single 25-feet tall tree can reduce annual heating and cooling costs of a typical residence by 8 to 12 % ($10-25) in San Diego, California. Similarly, another study (Chagolla et al., 2013) applied EngeryPlus simulations in Morelos, Mexico, demonstrating that tree shading reduced indoor temperatures by up to 4°C and achieved a 76.6% reduction in cooling energy demand. Additionally, a study in Abu Dhabi (Al-Sallal & Al-Rais, 2011), simulated the integration of vegetation such as shade trees, green roofs, and grass cover. These strategies reduced cooling energy use by up to 24% and fan operation by 27%. More recently, a study (Zhu et al., 2022) proposed a morphological framework for designing green infrastructure, emphasizing that tree placement in hot-humid climates can substantially lower cooling demand. Another study using parametric simulations in Canadian cities (Akbari & Taha, 1992) showed that increasing neighborhood vegetation and building albedo can reduce residential heating energy by up to 10% and can reduce cooling energy by up to 40% in urban areas, translating into substantial annual cost savings, with variations across cities and housing types. Another study (Hwang et al., 2016) simulated tree shading across four U.S. cities employing EnergyPlus as a means to evaluate the effect of a single shade tree upon a model having a floor area of 200 m^2 in four U.S. cities, and demonstrated that a large tree on the west could decrease annual energy costs by up to 160 kWh in southern cities with longer cooling seasons. All these simulation-based studies highlight the energy savings are achievable through trees.

Experimental and Empirical Studies. Controlled experiments and empirical analyses provide direct evidence of the impact of trees on A/C usage. A study (Laband & Sophocleus, 2009) conducted a field experiment in Beauregard, Alabama, comparing two identical buildings, one in full sun and the other shaded by trees. Results showed that the unshaded building required 2.6 times more electricity for cooling than the building in full shade, **illustrating the substantial local cooling benefits that trees can provide under ideal shading conditions**. Another study (Donovan & Butry, 2009) used household electricity billing data from 460 single-family homes in Sacramento, California, to statistically estimate electricity savings attributable to tree shade, confirming significant reductions in summertime residential cooling demand. Another study (Pandit & Laband, 2010), based on a sample of 160 residences in Auburn, Alabama, found that, in summertime, energy savings are maximized by having dense shade. Another study (Morakinyo et al., 2013) found that the indoor–outdoor temperature was higher during the day (ranging from 0.2 °C to 5.4 °C) for unshaded building and not more than 2.4 °C for the tree-shaded

building. These empirical studies validate energy simulation outcomes, providing evidence that tree shade decreases household energy consumption (or indoor air temperatures).

Large-Scale Urban Forestry Programs. Beyond individual buildings, large-scale urban forestry programs offer insight into the energy impacts of trees. The Sacramento Shade program, a prominent initiative in the US, has been extensively evaluated in a study (Ko et al., 2015) that monitored 22-years of post-planting survival, growth, and energy saving performance of shade trees in Sacramento, California. **The study found that only 34% of the trees originally delivered (or 42.5% of those confirmed planted) were still alive after 22 years, and that the average number of program trees per property declined from 3.1 to 1.3. Consequently, annual cooling energy savings per property reached only 22.7% of the 30-year projection, with a simulated saving of 80 kWh per tree, compared to the 153 kWh per tree originally projected.** Findings confirmed that lower survivorship was the major factor affecting lower cooling savings. In another study, the same author (Ko, 2018) synthesized evidence across North America, highlighting the effectiveness of tree planting for residential energy conservation, while also noting challenges related to tree survival rates, maintenance, and equity of distribution, highlighting that energy savings widely varied from 2.3% to 90% (cooling) and 1% to 20% (heating), **depending on the study scale and local conditions. This variability reflects the same contrast observed between statewide averages and controlled building-scale experiments, where shading effects can be substantially greater under ideal conditions**. These large-scale evaluations illustrate the system-level benefits and practical considerations of urban tree planting programs.

AI for segmenting trees. Recent advances in computer vision have enabled more precise quantification of urban vegetation by focusing not only on generalized greenness indices, but also on the explicit detection and segmentation of individual trees. Traditional approaches, such as the *Normalized Difference Vegetation Index* (NDVI) (Rouse et al., 1974) or *Green View Index* (GVI) and *Green Space Similarity Index* (GSSI) extracted from Google Street View Imagery (Mahajan, 2024), provide a broad characterization of vegetation cover but do not distinguish between vegetation types or isolate trees. By contrast, AI methods have been developed to segment and delineate tree crowns directly from aerial/satellite imagery. For example, authors (Bosch, 2020; L. Yang et al., 2009) introduced *DetecTree*, an open-source tool for tree detection from aerial imagery, while another author (Weinstein et al., 2019) applied semi-supervised deep learning to identify individual tree crowns in RGB imagery. Building on these advances, the *DeepForest* package (Weinstein et al., 2020) operationalized deep neural networks for large-scale tree crown delineation using RGB data, making tree segmentation more accessible for ecological and urban studies. More recently, foundation models for segmenting objects in any imagery, such as Meta's *Segment Anything Model* (Ravi et al.,

2024), have shown potential to further automate and generalize the task of object-level segmentation, including urban trees, across diverse imagery sources. These AI-based approaches represent a methodological shift from indirect proxies of vegetation to specific detection of trees, allowing fine-grained analysis of how tree canopy and coverage influence environmental outcomes, such as A/C usage.

1.2 Research gap and question

The reviewed literature demonstrates strong evidence that trees reduce indoor cooling loads (i.e. A/C usage) through shading and microclimatic regulation, with consistent findings across simulation studies, controlled experiments, and large-scale urban forestry programs. Based on these studies, the magnitude of savings varies by climate, tree placement, and building characteristics. However, several gaps were identified. *Most analyses are conducted at the building scale*, whereas neighborhood-level variations in tree canopy and their distributional impacts on cooling demand remain underexplored. The *majority of work comes from high-income regions*, where A/C adoption is widespread and tree-planting programs are supported by substantial institutional investment. *Little is known about how these interactions unfold in low-income, tropical contexts*, where A/C access itself is strongly shaped by socio-economic inequality. Third, while remote sensing has informed several urban forestry assessments, the *use of AI-based canopy detection methods to quantify neighborhood-scale tree coverage in relation to A/C usage has yet to be applied* in this field. This study addresses these gaps by focusing on a hot Honduran city, where A/C adoption is uneven and influenced by socio-economic conditions. By combining AI segmentation techniques to detect tree canopy with census-based neighborhood A/C usage data, the research evaluates how urban greenery influences cooling demand in a context where both environmental and social vulnerabilities are pronounced. The research question that guides the current study is: *To what extent does urban tree canopy coverage influence the use of A/C across diverse neighborhoods in the context of a hot Honduran city?* This approach not only extends the geographical and socio-economic scope of existing literature but also offers insights into how nature-based solutions like trees in cities can be leveraged to promote less A/C reliant communities in low-income tropical settings.

2. Methodology

This study focuses on neighborhoods of San Pedro Sula. This city is the largest metropolitan area in Honduras and one of the fastest growing and hottest urban agglomerations in Central America (see *Figure 1*). With a population nearing 2 million inhabitants, San Pedro Sula faces increasing challenges related to urban heat and uneven access to green infrastructure.

Figure 1. Satellite image of San Pedro Sula taken from Google Earth (2025).

To investigate the distribution of tree canopy and its relationship to neighborhood-level air conditioning (A/C) usage, this research employed a multi-step analytical framework integrating various data sources and computational tools. A schematic overview of the methodology is provided in *Figure 2*. In summary, the methodology followed four main phases:

1. *Data Collection of Satellite Images*. Aerial images were collected for all neighborhoods in San Pedro Sula. Following a few-shot learning approach, a subset of these images was manually labelled to identify tree canopies.

2. *Model Training and Tree Canopy Segmentation.* A pre-trained deep learning model from LandingAI was retrained using the labelled images. The retrained model was then used to automatically segment tree canopies across all neighborhoods in San Pedro Sula.

3. *Data Integration.* The resulting geospatial dataset of tree coverage was merged with additional datasets, including building footprints from OpenStreetMap and A/C usage data from census records. From this, the tree-to-building ratio for each neighborhood was calculated.

4. *Statistical Spatial Analysis.* Finally, spatial regression analyses were conducted to evaluate the influence of tree coverage, tree-to-building ratio and other covariates on neighborhood-level A/C usage.

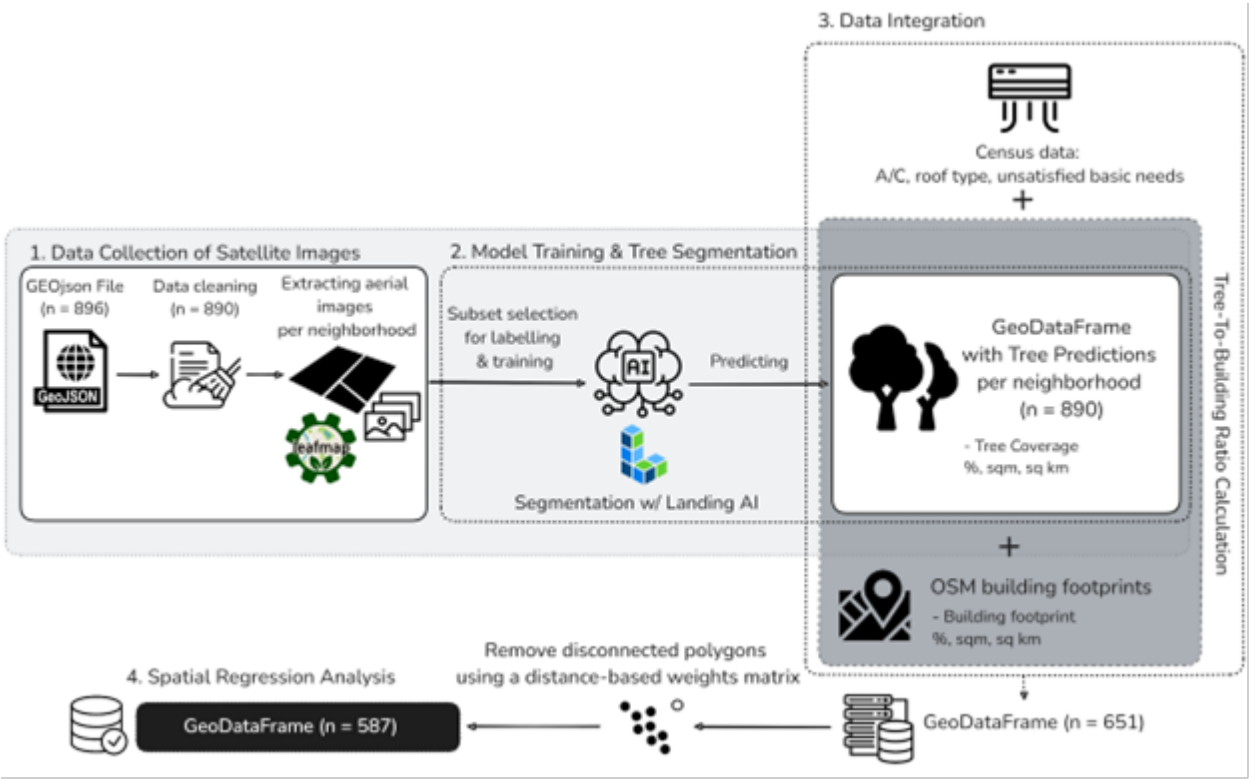

Figure 2. Multi-step analytical framework adopted in this study.

2.1 Data Collection of Satellite Images

As a starting point, neighborhood boundaries (i.e. polygons) were obtained from the National Territorial Information System of Honduras (SINIT, 2025), which provided official shapefiles delineating each neighborhood in San Pedro Sula, available as a GEOjson as downloadable file. According to SINIT's data (see *Figure 3*), the Metropolitan Zone of San Pedro Sula comprises 896 distinct neighborhoods, each represented by a separate polygon in the spatial GEOjson dataset.

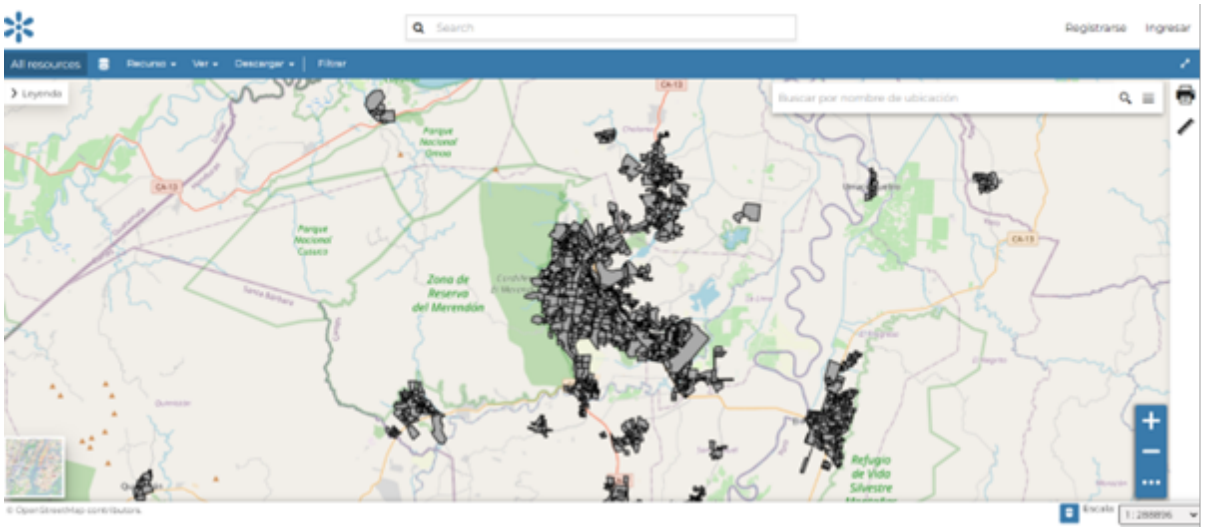

Figure 3. Neighborhood boundaries of San Pedro Sula, as defined by SINIT (2025).

The GEOjsonfile was imported into a GeoDataFrame using GeoPandas within a Google Colab environment (Google, 2025), where the data was explored, cleaned, and standardized to the WGS84 coordinate system (EPSG:4326). The neighborhood polygons were inspected and validated to ensure the spatial framework's integrity, as it would serve as the foundation for all subsequent analyses. During the cleaning process, four polygons were removed due to duplicated ID numbers, and two additional polygons, representing non-residential areas (*Ramon Villeda Morales Airport* and *Campisa Natural Park*), were also excluded. After these steps, the resulting GeoDataFrame contained 890 neighborhoods (see *Figure 4*).

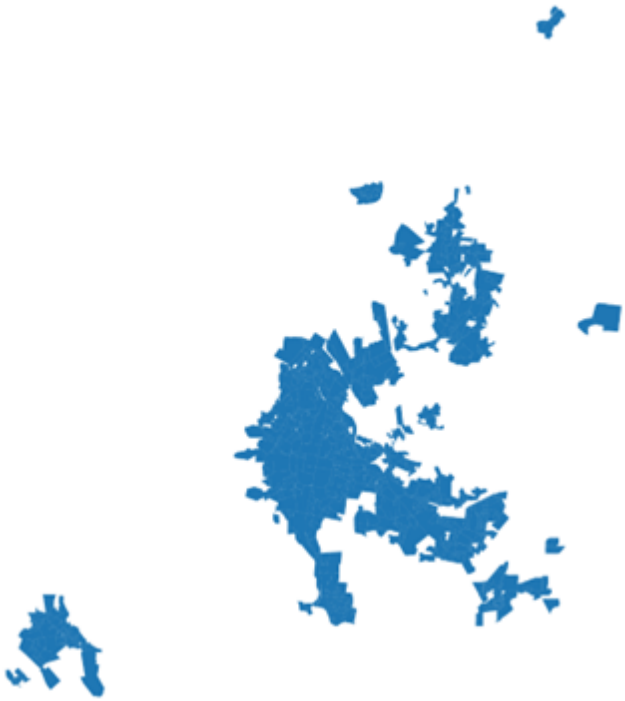

Figure 4. GeoDataFrame containing only 890 neighborhoods.

Then, the process employed *leafmap.Map()* and *leafmap.map_tiles_to_geotiff()* function within the *leafmap* package (Wu, 2021), which enables visualizing, downloading high-resolution aerial base maps (such as satellite imagery tiles) and saving them as georeferenced TIFF files. For each neighborhood polygon in San Pedro Sula's GeoDataFrame, the bounding box was calculated, and *leafmap* was used to retrieve a corresponding clipped raster image. As illustrated in *Figure 5* below, each image was downloaded at a high zoom level (zoom = 19) to ensure sufficient detail for subsequent analyses. The looped workflow systematically iterated through all neighborhood polygons in the GeoDataFrame and generated one TIFF file per neighborhood. This ensured that the imagery was spatially tailored, with each raster precisely aligned to the corresponding neighborhood boundary. The entire process was automated within the Colab notebook, using a combination of *GeoPandas* to extract geometry bounds and *Leafmap* to perform the tile download and raster generation. The resulting dataset consisted of 890 aerial images, which collectively covered the 890 neighborhoods of San Pedro Sula. This targeted approach avoided the need to manually handle large, unbounded raster scenes and reduced data storage requirements by limiting downloads strictly to the extent of each neighborhood. Moreover, it ensured that each image was directly usable for subsequent tasks, such as segmentation of individual trees using the LandingAI API (see Subsection 2.2) and cross-referencing with neighborhood-level features like A/C usage and unmet basic needs derived from census data (see Subsection 2.3).

Figure 5. Neighborhood polygon highlighted in red, displayed on an aerial image retrieved using the *Leafmap* package.

Given the extensive number of neighborhood images, a subsequent step was performed to identify a reduced, yet diverse, set of representative images that will be used for training the LandingAI deep learning model (see Subsection 2.2). For this purpose, each image was processed to extract numerical features capturing its visual and physical characteristics. These included normalized color histograms (96 features across the RGB channels) and the original width and height of each image (2 features), resulting in a 98-dimensional feature vector for each raster. These feature vectors were standardized using *Scikit-learn* package (Pedregosa et al., 2011) and its functions like *StandardScaler* for scaling, *PCA* for dimensionality reduction, and *KMeans* for clustering/grouping similar images. To select actual representative images rather than abstract centroids, a medoid approximation was performed; in other words, for each cluster, the real image closest in feature space to the cluster centroid was chosen.

2.2 Model Training and Tree Canopy Segmentation

Using LandingAI's platform (called LandingLens), a subset of representative aerial images was manually labelled to delineate tree canopies. LandingLens is a cloud-based, low-code platform developed by LandingAI for building, training, and deploying custom computer vision models (LandingAI, 2025). It offers automated image splitting and labelling tools, streamlining the model development process. LandingLens was selected for its user-friendly interface, which facilitated efficient image labelling and model training without the need for extensive infrastructure setup. The platform has also been successfully applied in other scientific domains (Anilturk et al., 2023; Hamdan et al., 2023).

Labelled images served as ground truth for training and validating the deep learning model. The dataset was divided into a *Train* and *Validation* set. The *Train* set was used to teach the model how to recognize patterns and objects of interest, while the *Validation* set (also referred to as the *Dev* set or *Development* set) was used to evaluate the model and monitor its performance. The *Validation* set plays a key role in preventing overfitting, a common issue where the model memorizes the training images instead of learning the underlying features needed to generalize to new data. This approach follows standard deep learning practices, where labelled datasets are typically split randomly with 80% assigned to training and 20% to validation. Model performance was evaluated by comparing predicted masks against the manually labelled ground truth using several metrics:

- *Confidence threshold:* it indicates the minimum confidence score the model must assign to a prediction in order for it to believe that its prediction is correct. Typically, a lower confidence threshold means that you will see more predictions, while a higher confidence threshold means you will see fewer. When LandingAI creates a model, it selects the confidence threshold with the best F1 score for all labelled data.
- *Confusion matrix:* it counts ground truth labels versus model predictions. The y-axis represents each ground truth label. The x-axis represents each possible model prediction. Each cell shows the count of instances that correspond to a particular ground truth class-predicted class pair.
- *Precision:* it answers the natural language question, *"When the model predicts Class A, how often is it correct?"* The Precision score for a class is the percentage of instances that the model correctly predicted the class out of all instances that the model predicted the class.
- *Recall:* it answers the natural language question, *"Of all the Class As in the dataset, what percent of them are found by the model?"* The Recall score for a class is the percentage of instances that the model correctly predicted the class out of all actual instances of the class.
- *Intersection over Union (IoU):* it measures the accuracy of the model by measuring the overlap between the predicted and actual masks in an image. A higher IoU indicates better agreement between the ground truth and predicted mask.

After training and validating, predictions (i.e. segmentations) were generated for all 890 neighborhoods using a looped batch-processing script. In this script, each aerial image was passed through the model to produce a tree canopy segmentation mask, which was then saved for further geospatial analysis. This was accomplished using LandingAI's cloud-based inference API, which enables fast and scalable deployment of computer vision models. The prediction workflow was implemented in Python using the *landingai* SDK. First, aerial images were loaded using the *PIL.Image* library (Clark, 2025). Each image was then passed to the LandingAI model endpoint, which returned a set of pixel-wise predictions indicating tree canopy presence.

Since the predicted tree canopy masks were initially generated in image pixel coordinates, they were reprojected to match the coordinate reference system (CRS) of the original aerial imagery. This reprojection step (performed within the batch-processing loop) ensured spatial consistency between the model outputs and other geospatial datasets used in subsequent analyses (see Subsection 2.4). To enable pixel-based coverage calculations, the reprojected polygons were rasterized into binary masks in image coordinates using the Python library *Rasterio* (Gillies, 2013). These masks served as the basis for computing the proportion of tree-covered pixels within each neighborhood boundary. As illustrated in *Figure 6*, tree canopy masks and neighborhood boundaries were visually inspected using overlay plots to verify spatial alignment and segmentation quality. This step helped validate both the model's predictions and the reprojection process, ensuring no systematic errors occurred during transformation.

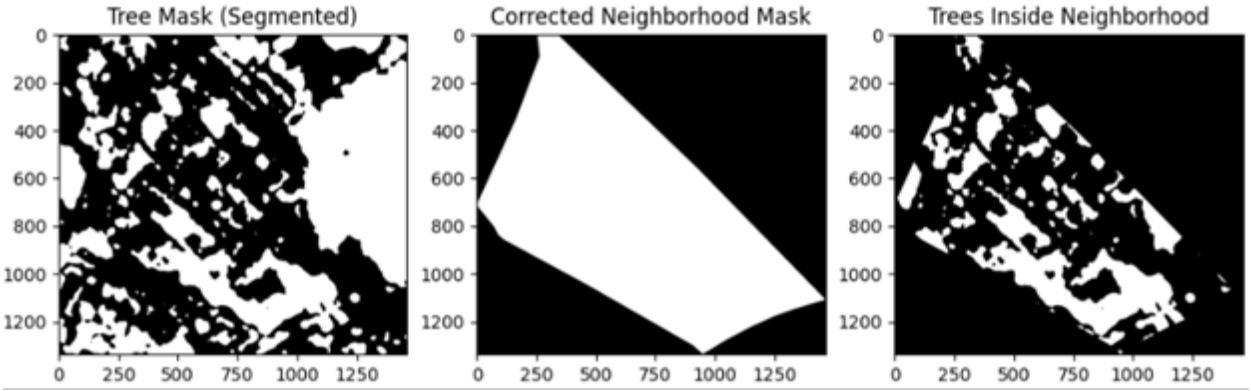

Figure 6. Tree canopy masks and neighborhood boundaries overlaid and visually inspected with *Rasterio*.

Within the same looped batch-processing script, tree canopy coverage (expressed as both *percentage* and *square meters*) was calculated for each neighborhood by measuring the extent of tree canopy pixels within each boundary mask. These coverage metrics were later used as key features in the spatial regression analysis (see Subsection 2.4).

2.3 Data Integration

Before performing the statistical spatial analysis, a data integration step was carried out. Tree coverage predictions from LandingAI's model, which provide estimated coverage for each neighborhood in San Pedro Sula, were merged with other external datasets. These included census-based variables (i.e., air conditioning usage, roof type) and OpenStreetMaps (OSM) data for calculating the tree-to-building ratio per neighborhood. All spatial operations and data joins were conducted using SINIT's GeoDataFrame containing neighborhood-level polygons. During this integration process, the number of neighborhoods in the GeoDataFrame was reduced from 890 to 651. This reduction occurred since many neighborhoods in OSM lacked building footprints, despite the existence of actual buildings, which is an expected limitation of open-source platforms especially for low-income urban contexts. Consequently, neighborhoods without building data from OSM were excluded from the final spatial analysis. External datasets are the following:

- *Census data*. Socioeconomic and housing characteristics, including A/C ownership, roofing material, and indices of Unsatisfied Basic Needs (NBI), were obtained from the most recent national census provided by the Honduran National Statistics Institute (INE, 2025). The data were available as a downloadable CSV file, containing counts per neighborhood for each variable. These tabular datasets were spatially joined to the GeoDataFrame using neighborhood identifiers, enriching each polygon with relevant demographic attributes.

- *OSM Building Footprints*. Individual building footprints across San Pedro Sula were extracted using the *OSMNX* library (Boeing, 2025), which interfaces with OSM data. OSM is a free, open map database updated and maintained by a community of volunteers via open collaboration (Haklay & Weber, 2008) . This dataset was spatially joined to the neighborhood polygons and later used to calculate the tree-to-building ratio at the neighborhood scale, a critical feature for assessing urban greenery relative to impervious surfaces.

2.4 Statistical Spatial Analysis

When working with spatial data and applying regression models, potential spatial autocorrelation should be considered. Positive spatial autocorrelation occurs when observations in areas that are geographically close tend to have similar values, meaning

the variable is not independently observed across space. If this spatial dependence is ignored, for example, by fitting an Ordinary Least Squares (OLS) regression model, the standard assumptions of classical regression, particularly the independence of errors are violated. As a result, the usual estimates of standard errors become biased, leading to incorrect statistical inference (Anselin, 1988). Therefore, for the analysis of these data, tests for spatial autocorrelation will be conducted, and alternative models that account for this spatial dependence will be considered.

The spatial weights matrix is used to represent the spatial structure of the dataset under analysis (Getis & Aldstadt, 2004). It is typically an *n* × *n* matrix, where each element *wij* indicates the spatial relationship between regions i and j. A common specification is binary, where $w_{ij} = 1$ if area i is considered a neighbor of area j and 0 otherwise. Different criteria can be used to define whether two regions are neighbors. For example, under the Queen contiguity criterion, two regions are considered neighbors if they share at least one point on their physical borders. Alternatively, a distance-based criterion can be applied, where two regions are neighbors if the distance between their centroids is less than or equal to a specified threshold. The centroid of a region is the geometric center of its shape, typically calculated as the average of all its coordinate points. For polygons, this is the center of mass assuming uniform density. In practice, the weights matrix is often row standardized so that the weights in each row sum to 1. This transformation converts raw weights into relative weights, ensuring comparability across regions with different numbers of neighbors. As a result, each region's set of neighbors exerts an equal combined influence, regardless of how many neighbors it has.

The spatial lag operator functions similarly to the lag operator in time series analysis; however, in the spatial context, there are multiple directions along which autocorrelation can occur. For a variable y, its spatial lag, Wy, is the product of the spatial weights matrix by the vector of observations of the variable, so that:

$$Wy_i = \sum_{j=1}^{n} \quad w_{ij}y_j, \qquad \text{for } i = 1, \ldots, n$$

Each Wy_i represents a kind of weighted average of the values of the variable in neighboring regions. When the spatial weights matrix W is row-standardized (i.e., each row sums to one), the spatial lag behaves like a local smoothing of the neighboring values.

Several statistics have been developed to test for the presence of global spatial autocorrelation in the data, such as Moran's I (Moran, 1948) and Geary's C (Geary, 1954). The most widely used is Moran's I, whose null hypothesis states the absence of spatial autocorrelation. A significantly positive value of the test statistic indicates the presence of positive spatial autocorrelation, meaning a clustering of similar values of the variable in

neighboring regions. In contrast, a significantly negative value indicates negative spatial autocorrelation, where neighboring regions tend to have dissimilar values, for example, high values surrounded by low values and vice versa. Geary's C is an alternative measure that also detects spatial autocorrelation but is more sensitive to local differences between neighboring values. While Moran's I is a measure of global similarity, Geary's C focuses on local dissimilarity. In this case, values of C near 1 indicate spatial randomness, values below 1 suggest positive spatial autocorrelation, and values above 1 indicate negative spatial autocorrelation, i.e., neighboring regions tend to have dissimilar values.

Let y be the response variable in our dataset, and assume that a set of covariates is observed for n neighborhoods or areas, yielding a matrix of observations, X, of dimension $n \times k$. Spatial autocorrelation in such data is commonly addressed through spatial autoregressive models that incorporate spatial dependence explicitly into their structure. The spatial lag model (Anselin, 1988) assumes that the spatial autocorrelation is directly observed and includes the spatial lag of the response variable, Wy, as a covariate in the regression structure:

$y = X\beta + \rho Wy + \varepsilon, \varepsilon \sim N(0, \sigma^2 I)$, where β is the vector of coefficients of the variables in X, ρ the spatial parameter that measures the strength of the spatial dependence in the response variable and ε is the vector of Gaussian error terms.

The spatial error model (Anselin, 1988) assumes the spatial autocorrelation is unobserved and is contained in the residuals of the regression model. It is formulated as:

$$y = X\beta + u, \qquad u = \lambda Wu + \varepsilon, \qquad \varepsilon \sim N(0, \sigma^2 I)$$

where λ is the spatial parameter accounting for the spatial dependence in the error term.

The spatial Durbin model (LeSage & Pace, 2009) extends the spatial lag model by including spatially lagged values of the covariates in addition to the lagged dependent variable. The model is given by: $y = X\beta + \rho Wy + \theta WX + \varepsilon, \varepsilon \sim N(0, \sigma^2 I)$,

where θ is the vector of spatial parameters for the covariates. This formulation accounts for the possibility that covariates themselves may exhibit spatial autocorrelation, and that their neighboring values may influence the response variable as well.

The aforementioned models assume a Gaussian response. For spatially referenced count data, it is common to account for overdispersion and spatial correlation through hierarchical models incorporating spatial random effects. Two widely used spatial generalized linear mixed models for this purpose are the Besag–York–Mollié (BYM) model and the Leroux conditional autoregressive (CAR) model, which capture the spatial autocorrelation by including random effects in the regression structures.

The Leroux model (Leroux et al., 2000) specifies a Conditional Autoregressive (CAR) distribution on the random effects, so that: $g(\mu) = O + X\beta + \phi$
where $g(.)$ is the logarithm function and the logistic function for Poisson or binomial responses, respectively. O is a vector of known offsets and ϕ is a set of random effects following the conditional distribution (Lee, 2013):

$$\phi_k|\phi_{-k} \sim \mathrm{N}\left(\frac{\rho\sum_{i=1}^{n} w_{ki}\phi_i}{\rho\sum_{i=1}^{n} w_{ki}+1-\rho}, \frac{\tau^2}{\rho\sum_{i=1}^{n} w_{ki}+1-\rho}\right)$$

where $-k$ represents the set of all the random effects excluding the $k-$ th one, w_{ki} represents the spatial weight that specifies the neighborhood structure between regions k and i and the parameter ρ is the spatial dependence parameter. Values of ρ close to one indicate strong spatial autocorrelation, whereas values near zero suggest little to no spatial autocorrelation. In addition, τ^2 is the variance.

The BYM model (Besag et al., 1991), also known as the convolution model, decomposes the spatial random effect into two components: a structured spatial effect that captures autocorrelation between neighboring areas via an intrinsic CAR prior distribution, and an unstructured effect modeled as independent and identically distributed. If it is assumed that the response variable follows a count data distribution (e.g. Poisson, binomial), then the model is typically specified for the mean as: $g(\mu) = O + X\beta + \theta + \phi$

where θ is a set of Gaussian unstructured random effects, $\theta \sim N(0, \sigma^2)$, and ϕ are CAR distributed random effects following (Lee, 2013):

$$\phi_k|\phi_{-k} \sim \mathrm{N}\left(\frac{\sum_{i=1}^{n} w_{ki}\phi_i}{\sum_{i=1}^{n} w_{ki}}, \frac{\tau^2}{\sum_{i=1}^{n} w_{ki}}\right)$$

where all the terms are as before.

These models are specified within a Bayesian framework and are typically estimated using Markov chain Monte Carlo (MCMC) methods, an approach that is particularly suitable because the Leroux and BYM spatial models involve latent spatial random effects and complex hierarchical structures that make analytical solutions intractable. MCMC algorithms allow for efficient approximation of the posterior distributions of parameters, providing a flexible way to incorporate prior information and quantify uncertainty in spatial dependence.

As a post hoc complement to the spatial regression models, Local Indicators of Spatial Association (LISA) (Anselin, 1995) were used to investigate localized spatial relationships between A/C usage and environmental features. Specifically, the bivariate Local Moran's I statistic was employed to assess how values of a local variable (e.g., A/C usage per neighborhood) are associated with the spatial lag of a different variable (e.g., tree coverage in adjacent neighborhoods). This method enables the identification of spatial clusters—such as *High-High* (HH), *Low-Low* (LL), *High-Low* (HL), and *Low-High* (LH)—where statistically significant local patterns ($p < 0.05$) deviate from randomness. The analysis was performed using the *PySAL* package in Python (Rey & Anselin, 2007), and all variables were standardized (z-scores) prior to analysis. These cluster maps provide fine-grained spatial diagnostics that enrich the interpretation of global spatial regression results by pinpointing where environmental greening may influence A/C demand most acutely.

3. Results

This section presents the results of the tree canopy segmentation, data integration, and spatial statistical analysis. Subsection 3.1 details the performance of the deep learning model used for segmenting tree canopies and provides an overview of tree coverage across San Pedro Sula. Subsection 3.2 summarizes the geospatial features derived from external datasets, including building footprints and A/C usage. Finally, Subsection 3.3 presents the findings of the spatial regression analysis, which assessed the influence of tree-related metrics and other covariates on neighborhood-level A/C usage.

3.1 AI's Tree Canopy Segmentation Outputs

LandingAI's model employs a few-shot learning approach, requiring a minimum of 10 images for training. In this study, however, a stricter selection process was implemented to ensure both efficiency and representativeness. As described in Subsection 2.1, a clustering-based method (i.e., Kmeans) was used to identify a reduced yet diverse set of training images that captured the variation in urban form and vegetation across neighborhoods. This process resulted in a curated subset of 19 representative images (see *Figure 7*), which were then manually labelled to serve as ground truth labels.

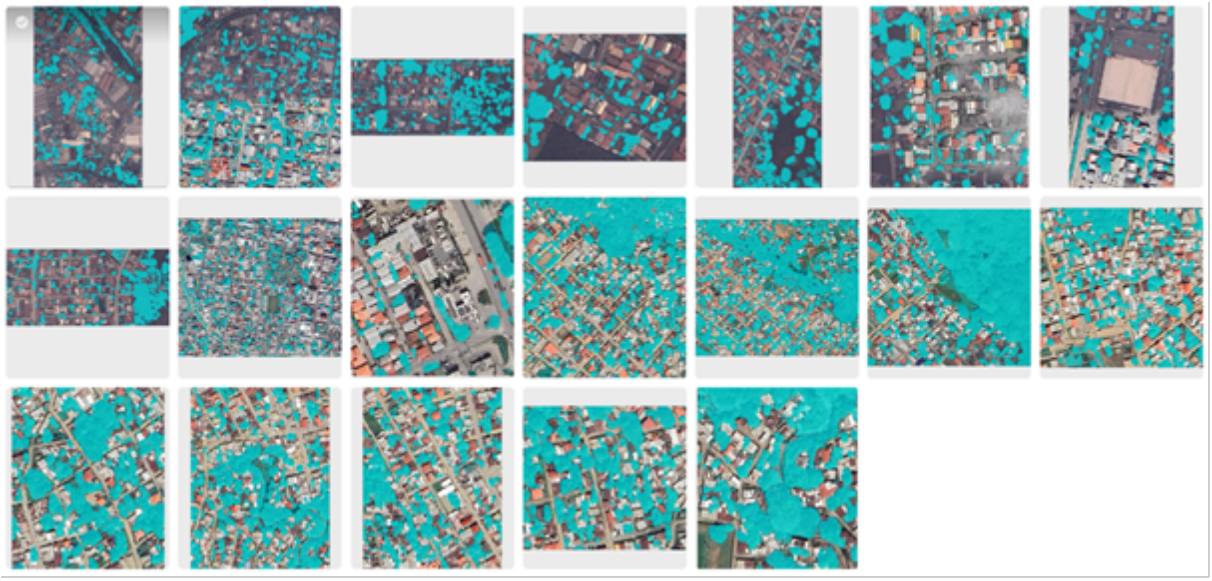

Figure 7. Subset of 19 labelled images used for training the LandingAI's computer vision model. Note: blue color indicates tree canopies.

To evaluate the performance of the tree canopy segmentation model, the dataset of 19 labelled images was divided into a *Training* set (15 images, 9.3 million labelled pixels; 78.9% of the dataset) and a *Validation* set (4 images, 2.1 million labelled pixels; 21.1% of the dataset). As shown in the *confusion matrix* within *Figure 8*, the model achieved an *IoU* of 69.5% on the training set and 64.2% on the validation set, indicating a reasonable degree of overlap between the predicted and actual canopy masks, with a modest decrease on unseen data. In terms of *recall*, which measures the model's ability to identify actual tree canopy pixels, the performance declined from 85.5% in training to 78.3% in validation, suggesting that the model missed more canopy pixels in the validation set. *Precision*, which assesses how often predicted canopy pixels were correct, remained relatively stable, decreasing only slightly from 78.8% in training to 78.1% in validation. Based on the best *F1 score* for all labelled data, LandingAI's model selected defined a confidence threshold of 0.79 for these predictions. *Figure 9*, *Figure 10*, *Figure 11 and Figure 12* below show, for all four neighborhoods within the *Validation* set, a comparison between the ground truth labelling, the prediction (i.e. segmentation) of LandingAI's model, the false negative pixels, and the false positive pixels.

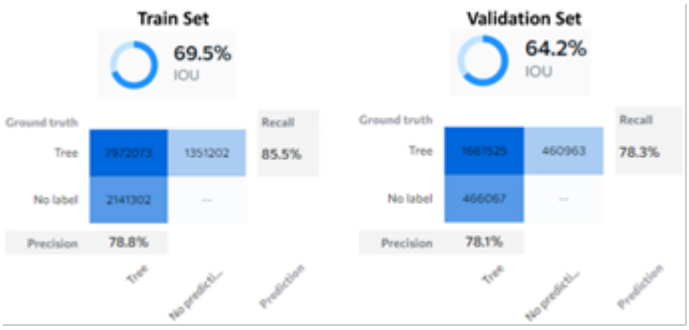

Figure 8. Confusion matrix for both Train and Validation sets.

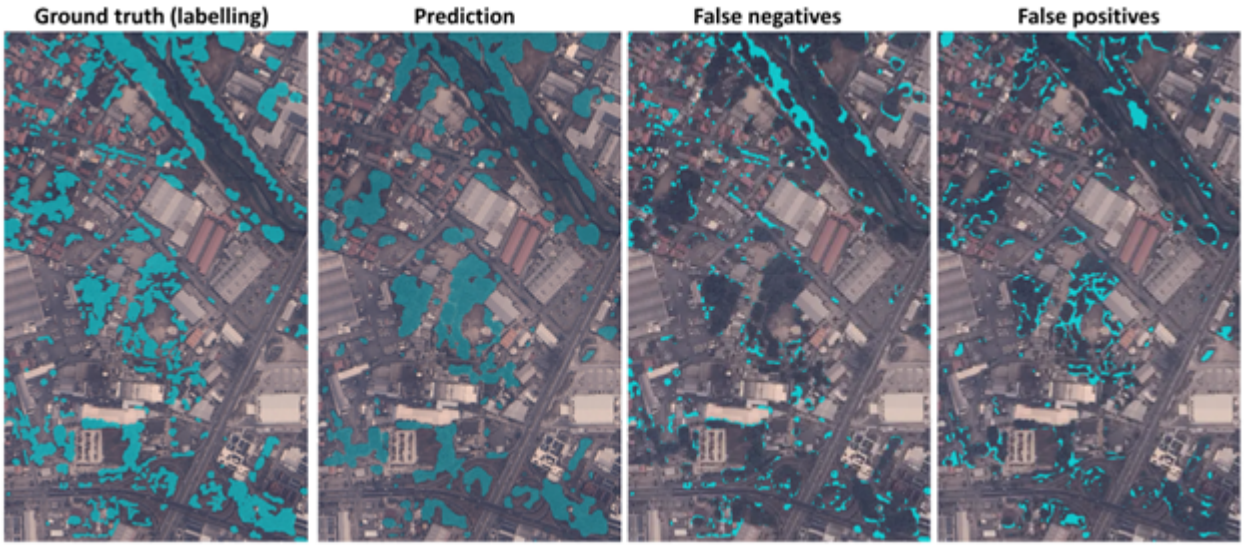

Figure 9. Comparison between the ground truth labelling and the prediction (i.e. segmentation) of LandingAI's model for neighborhood with ID number 274.

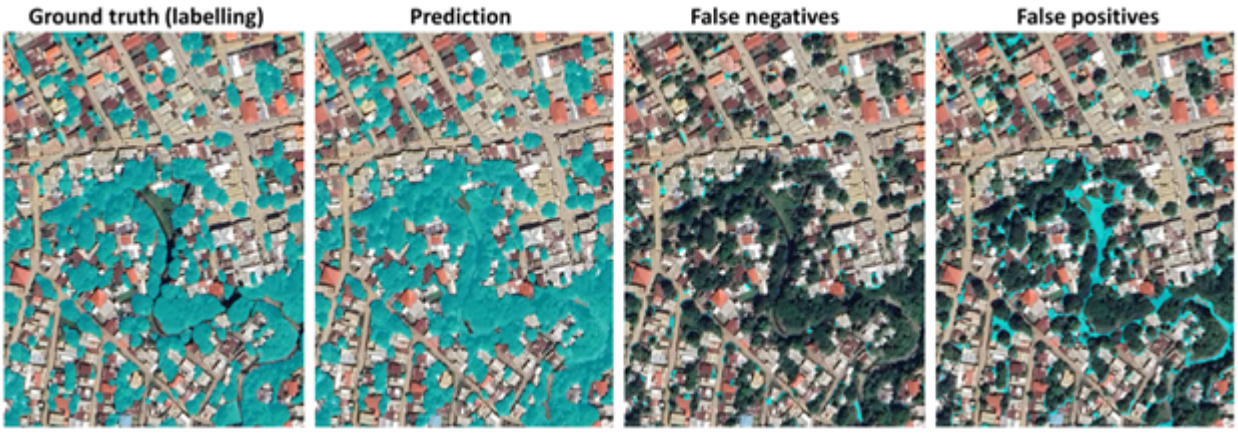

Figure 10. Comparison between the ground truth labelling and the prediction (i.e. segmentation) of LandingAI's model for neighborhood with ID number 19.

Figure 11. Comparison between the ground truth labelling and the prediction (i.e. segmentation) of LandingAI's model for neighborhood with ID number 40.

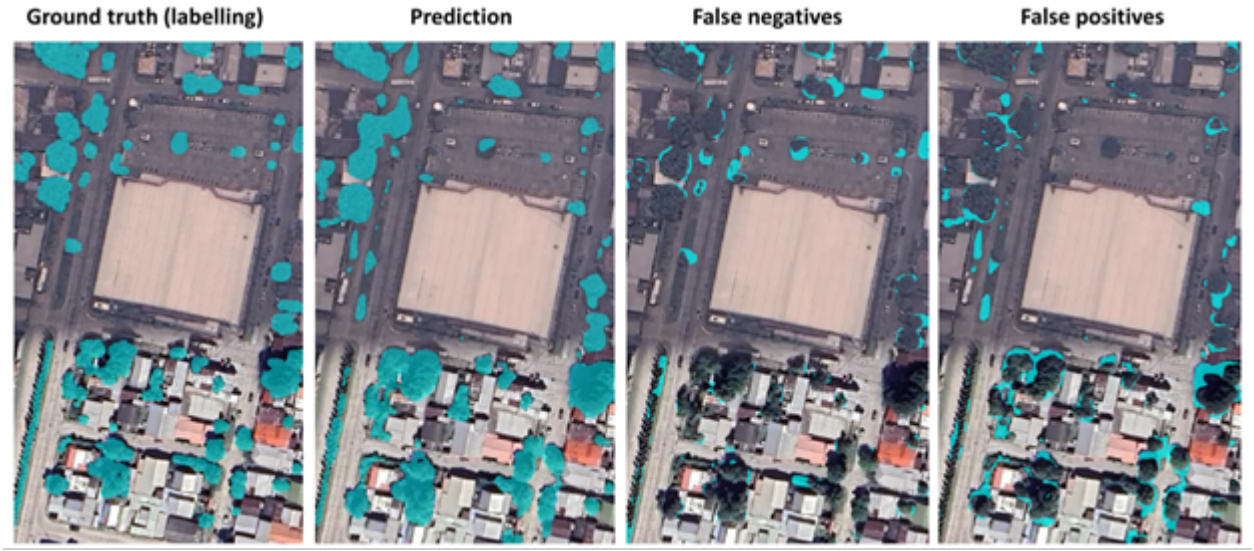

Figure 12. Comparison between the ground truth labelling and the prediction (i.e. segmentation) of LandingAI's model for neighborhood with ID number 266.

3.2 Tree Canopy Coverage in San Pedro Sula

Overall, based on tree canopy predictions from the LandingAI model developed in this study, approximately 75.26 km² of San Pedro Sula city is covered by trees. As illustrated in *Figure 13*, this value represents 44.8% of the city's total neighborhood-defined area (i.e., 75.34 km²), which amounts to 168.17 km², based on SINIT's GeoJSON file.

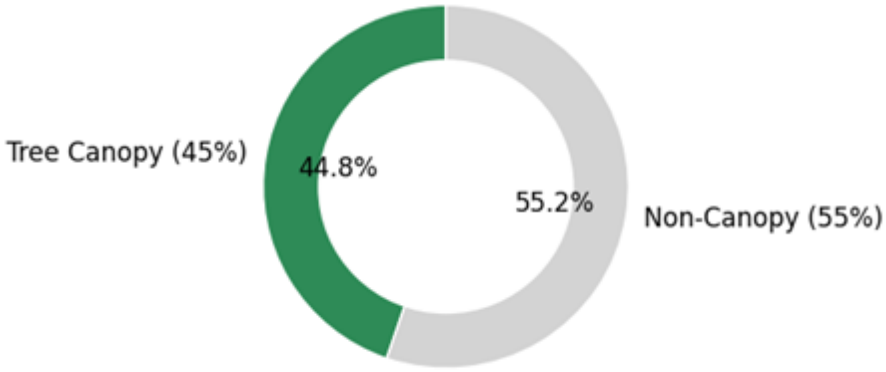

Figure 13. Total percentage of tree canopy coverage in San Pedro Sula.

3.3 Statistical Spatial Analysis

After aggregating tree canopy data at the neighborhood level, the resulting GEODataFrame was combined with additional datasets (i.e., household statistics from the Honduran INE, building footprints from OSM) to prepare for geospatial analysis. As described in Subsection 2.3, this integration produced a dataset of n = 651 neighborhoods. Following this, and as outlined in Subsection 2.4, isolated neighborhoods within the spatial weights matrix were removed based on the minimum distance required for each neighborhood (i.e., polygon) to have at least one neighboring polygon, as illustrated in *Figure 14*. This step reduced the dataset to n = 587 neighborhoods, with 1675 meters identified as the threshold distance ensuring every neighborhood has at least one neighbor. *Table 1* below describes summary statistics for all key features extracted from all data sources.

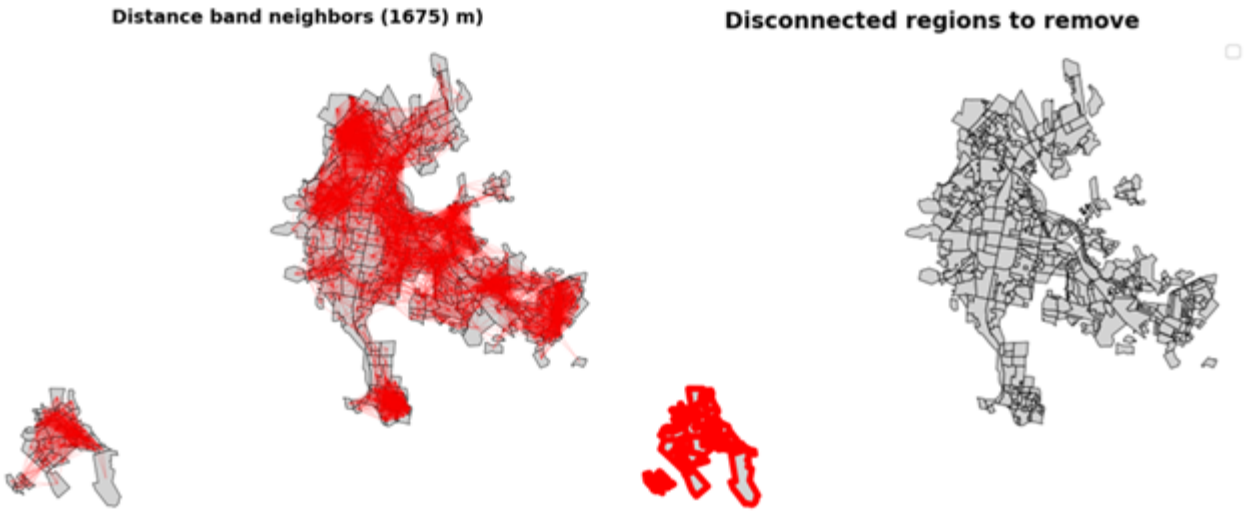

Figure 14. Minimum-distance spatial weights matrix (left) and polygons removed for lacking a neighboring polygon within 1675 meters (right).

Feature	Mean	Std.	Min.	50%	Max.
Tree Coverage (%)	34.32	20.47	0.09	29.58	98.68
Tree Area (km²)	0.08	0.15	0.0	0.03	1.48
Tree-to-Building Ratio	12.49	73.96	0.01	1.49	1144.32
Neighborhood Area (km²)	0.19	0.27	0.0	0.09	2.27
Building Footprint (%)	20.47	10.74	0.05	20.99	50.75
Building Footprint (km²)	0.03	0.05	0.0	0.01	0.34
A/C Usage (%)	33.15	29.63	0.0	23.08	100.0
A/C Usage (counts)	75.78	142.48	0.0	26.0	1474.0
Households with 0% UBI (%)	60.59	24.03	0.0	64.38	100.0
Households with 0% UBI (counts)	159.51	277.31	0.0	61.0	3345.0
Roof - Metal type (%)	77.28	25.75	0.0	87.7	100.0
Roof - Metal type (counts)	278.83	452.96	1.0	124.0	5384.0

Table 1. Summary statistics for all key variables extracted across data sources.

Histograms, illustrated in *Figure 15*, reveal distinct patterns of skewness across San Pedro Sula. A/C usage (%) (*pc_ac*) displays a strong right skew, with most neighborhoods reporting low adoption levels and a long tail indicating limited access to A/C in much of the city. The tree-to-building ratio (*tree_blt_r*) is also heavily right-skewed, with the majority of neighborhoods showing low ratios and only a few outliers having large tree canopy areas relative to built surfaces. Tree coverage (%) (*pc_tree_cv*) follows a right-skewed distribution, with most neighborhoods clustered between 20 and 40%, and relatively few areas showing high values, indicating an overall limited presence of green cover across the city. Households with no unsatisfied basic needs (%) (*pc_nbi0*) follows a left-skewed distribution, with most neighborhoods concentrated between 60% and 80%, and relatively few falling below 60%, indicating that while socioeconomic well-being is relatively moderate to high in many neighborhoods, a smaller number still exhibit signs low-income contexts. In contrast, households with metallic roofs (%) (*pc_met_rf*) are left-skewed, with most neighborhoods having high concentrations of metal roofing, typically associated with lower-income housing stock. The feature tree-to-building ratio (*tree_blt_r*) exhibited extremely high positive skewness (*skewness* = 11.498), indicating a heavy concentration of low values and a few extreme outliers; therefore, suggesting inspection and possibly log-transformation for further analyses.

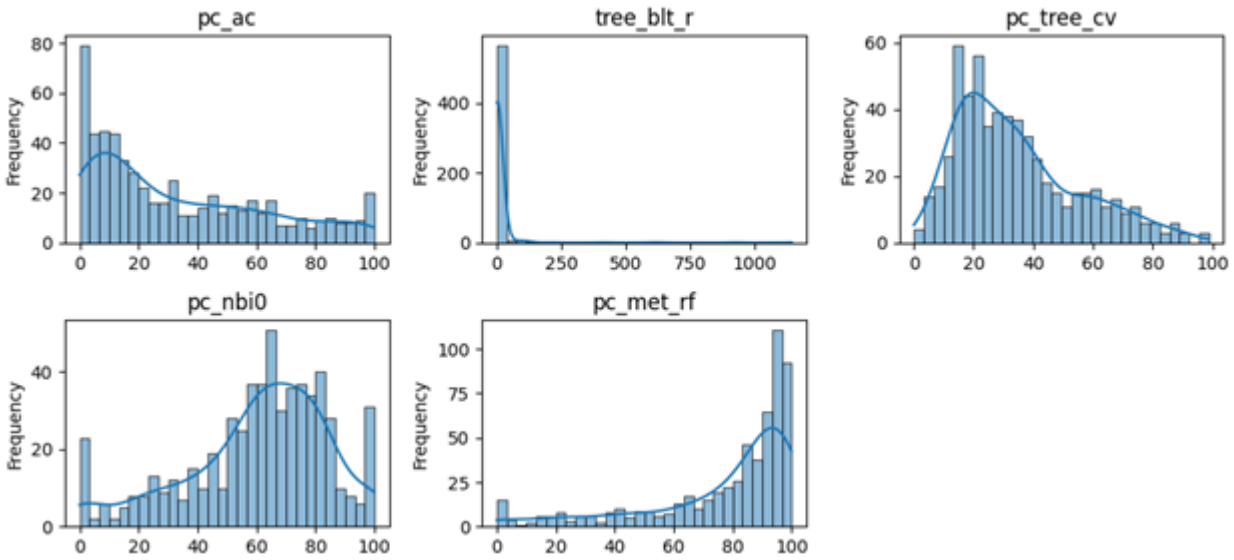

Figure 15. Histograms for key features: [pc_ac] A/C Usage (%), [tree_blt_r] Tree-to-Building Ratio, [pc_tree_cv] Tree Coverage (%), [pc_nbi0] Households with 0% UBI (%), and [pc_met_rf] Roof - Metal type (%).

Correlation analysis (*Figure 16*) reveals relationships among key neighborhood features in San Pedro Sula. A/C usage (%) (*pc_ac*) shows a positive correlation with households with no unsatisfied basic needs (%) (*pc_nbi0*, r = 0.42), suggesting that A/C access is more prevalent in higher-income areas. It also has a negative correlation with metal roof coverage (%) (*pc_met_rf*, r = -0.35), indicating that neighborhoods with poorer-quality roofing tend to have lower A/C usage. Additionally, tree coverage (%) (*pc_tree_cv*) and tree-to-building ratio (*tree_blt_r*) are negatively correlated with A/C usage (r = -0.13 and r = -0.065, respectively), suggesting that neighborhoods with higher tree cover and higher tree-to-building ratio are less reliant on A/C. Also, *pc_tree_cv* is also negatively correlated with *pc_nbi0* (r = -0.29), indicating that neighborhoods with more tree cover tend to have lower-income levels.

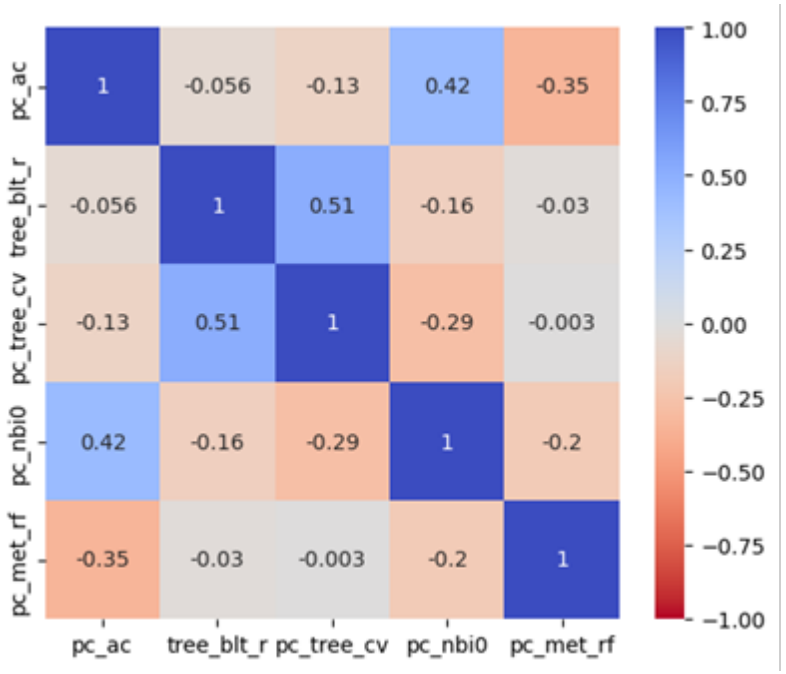

Figure 16. Correlogram showing Pearson's correlation values for: [pc_ac] A/C Usage (%), [tree_blt_r] Tree-to-Building Ratio, [pc_tree_cv] Tree Coverage (%), [pc_nbi0] Households with 0% UBI (%), and [pc_met_rf] Roof - Metal type (%).

3.3.1 Tree Canopy Coverage

As shown in *Figure 17*, the spatial distribution of tree canopy cover across San Pedro Sula illustrates a marked imbalance: neighborhoods near the city center tend to have lower tree density, while peripheral areas, particularly those adjacent to natural landmarks such as the *Sierra del Merendón* (west), *Campisa Natural Park* (north), and the *Jucutuma Lagoon* (east), exhibit higher levels of tree cover. After integrating additional data sources (n = 651), the analysis shows that tree canopy covers 34.32% of each neighborhood's area, with a mean tree-covered surface of 0.08 km², accounting for variations in neighborhood size.

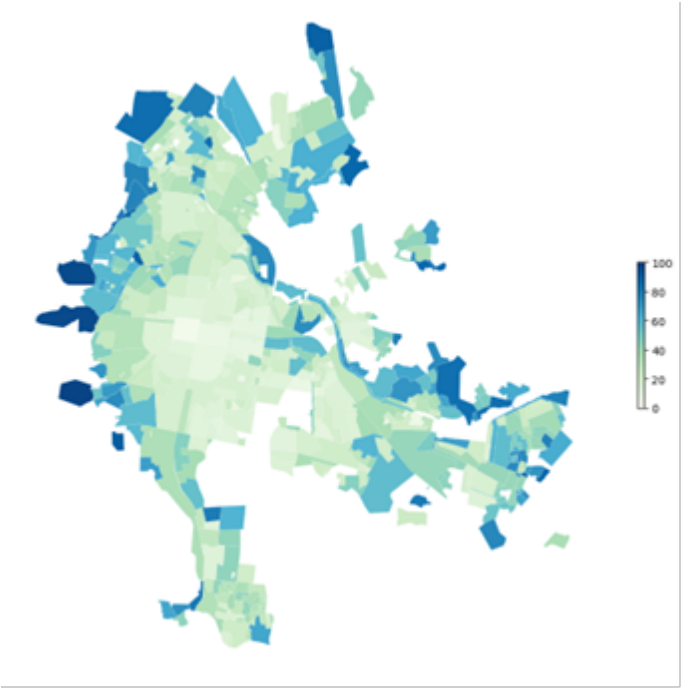

Figure 17. Spatial distribution of tree coverage (%) across San Pedro Sula

3.3.2 A/C usage

Based on census data from INE (n = 890), approximately 56,870 households in San Pedro Sula report having air conditioning, representing 26.14% of all households citywide. After integrating additional data sources (n = 587), the analysis indicates that, on average, 33.15% of households in each neighborhood use A/C, with a mean of 75.78 A/C-equipped households per neighborhood. However, the spatial distribution of households with A/C across San Pedro Sula reveals an imbalance. Neighborhoods on the western side of the city (i.e. especially those near the *Sierra del Merendón*) show a significantly higher concentration of A/C-equipped households, reflecting the generally higher-income conditions in these areas. To normalize distributions (previously shown in *Figure 15*), *pc_ac* was transformed using the natural logarithm, resulting in *log_pc_ac*, respectively. *Figure 18* illustrates the spatial distribution of A/C adoption across San Pedro Sula.

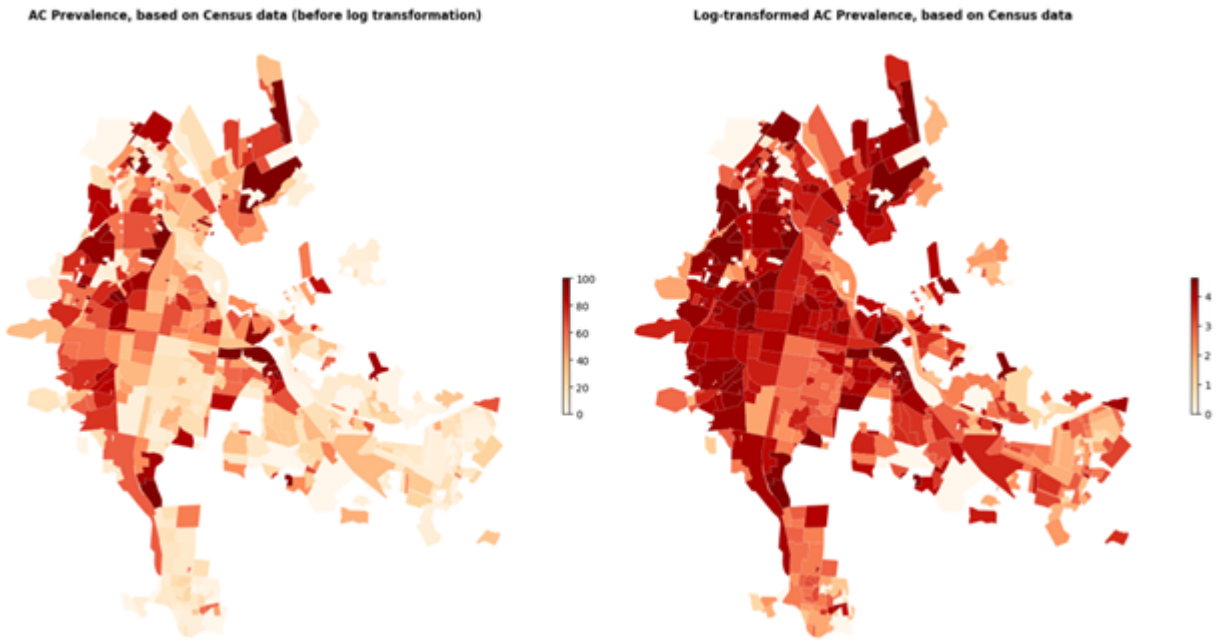

Figure 18. Spatial distribution of A/C usage across San Pedro Sula: left (before log-transformation) and right (after log-transformation).

3.3.3 Households with Unsatisfied Basic Needs

According to census data from INE (n = 890), approximately 129,301 households in San Pedro Sula report having no unsatisfied basic needs, accounting for 60.11% of all households in the city. After incorporating additional data sources (n = 587), the analysis shows that, on average, 60.59% of households in each neighborhood report no unsatisfied basic needs, with a neighborhood-level mean of 159.51 such households. This distribution, however, is uneven. Neighborhoods on the eastern side of the city (illustrated in darker red) tend to have a significantly lower number of households meeting all basic needs—indicating lower-income conditions in these areas. *Figure 19* illustrates the spatial distribution of these households across San Pedro Sula.

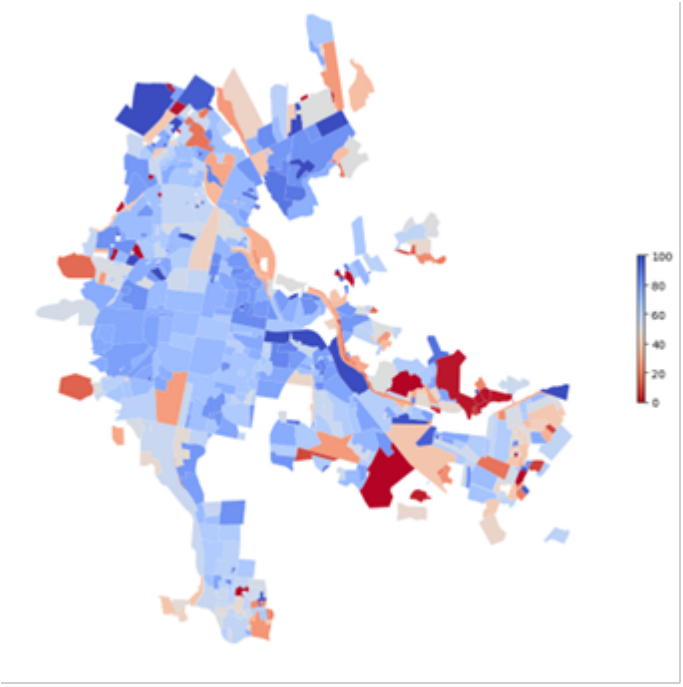

Figure 19. Spatial distribution of percentage of households with no unsatisfied basic needs (UBI) across San Pedro Sula.

3.3.4 Metal Roofs

According to census data from INE (n = 890), approximately 201,100 households in San Pedro Sula report having a metallic roof (i.e., zinc, aluminum-zinc), representing 84.03% of all households citywide. After integrating additional data sources (n = 587), the analysis reveals that, when averaged across neighborhoods, 77.28% of households per neighborhood have metallic roofs, with a mean of 278.83 such households per neighborhood. This distribution is also spatially uneven: neighborhoods on the eastern side of the city tend to have higher households with metallic roofs, a characteristic associated with lower-income housing. *Figure 20* illustrates the spatial distribution of these households across the city.

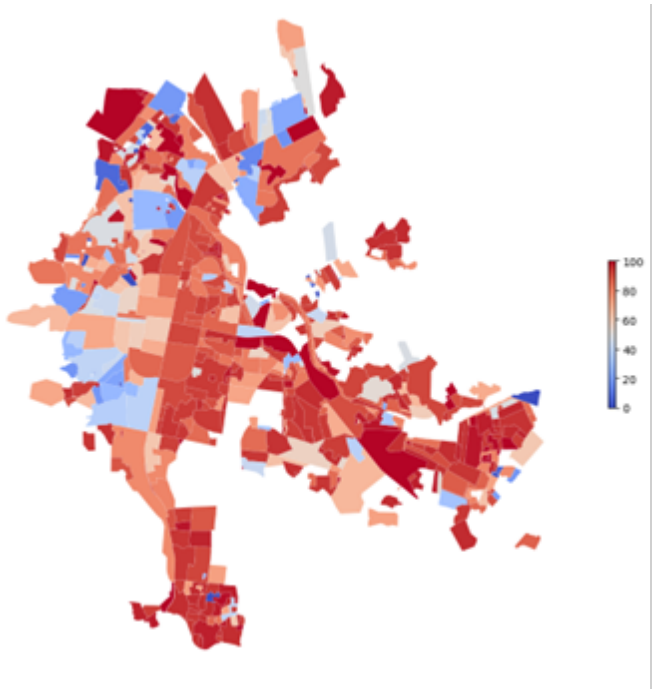

Figure 20. Spatial distribution of metal roofs across San Pedro Sula.

3.3.5 Tree-To-Building Ratio

In overall numbers, San Pedro Sula has a tree-to-building ratio of 2.64—meaning that across the city, for every 1 sq km of building footprint, there are approximately 2.64 sq km of tree canopy coverage. When averaging this ratio across individual neighborhoods (regardless of their size), the mean neighborhood-level tree-to-building ratio is 12.49. Outlier detection based on visual inspection of choropleth maps, as illustrated in *Figure 21*, revealed unusually high values in specific neighborhoods for *tree_blt_r* (values > 200). Spatial smoothing was subsequently applied to *tree_blt_r* by replacing the extreme values with their corresponding spatial lag averages. Post-smoothing visualization confirmed a reduction in extreme local variability while maintaining broader spatial trends. To normalize distribution (previously shown in *Figure 15*), the tree-to-building ratio feature was transformed using the natural logarithm, resulting in *log_tree_blt_r*. *Figure 21* also illustrates the spatial distribution of the log-transformed tree-to-building ratio, showing that the ratio increases in neighborhoods located near the urban periphery, where tree cover is more abundant. In contrast, neighborhoods closer to the city center tend to have lower ratios, likely due to higher urban density and limited space for vegetation.

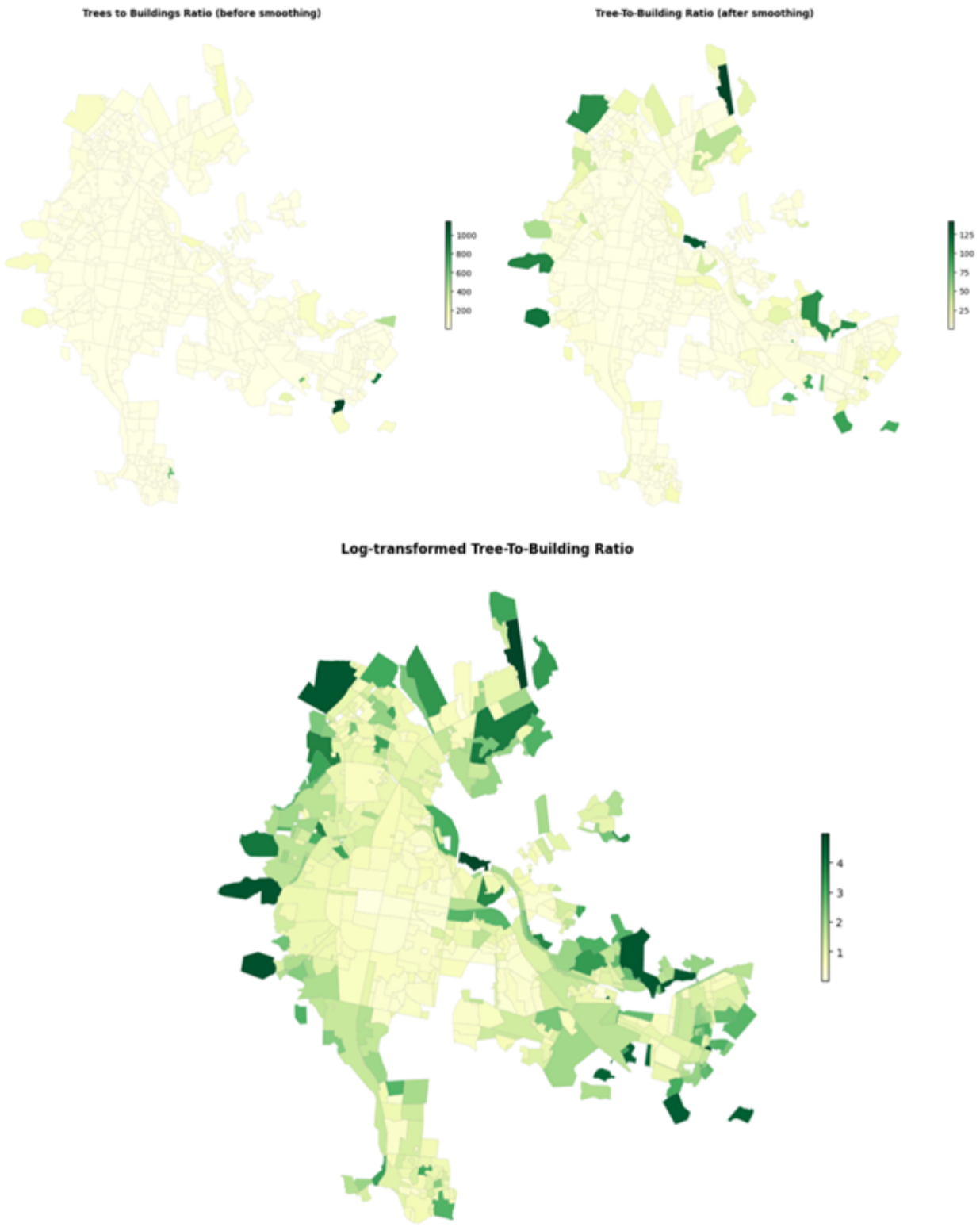

Figure 21. Spatial distribution of tree-to-building ratio across San Pedro Sula. Upper left (before smoothing), upper right (after smoothing), and below (after smoothing log-transformed).

3.4 Spatial Analysis

After exploring different options, the distance-based criterion has been selected for defining the spatial weights matrix, setting the threshold to the minimum distance that ensures every area is connected to at least one neighbor. However, as explained at the beginning of Subsection 3.3, in the original shapefile, several regions were located far from the main cluster of neighborhoods with non-zero constructed areas. This created a challenge when applying the distance-based approach since the required minimum distance became excessively large, resulting in some areas having too many neighbors and thereby reducing the ability to accurately capture spatial dependence. To address this issue, a number of regions were excluded from the analysis.

Spatial autocorrelation metrics were computed for the five key features using both Moran's I and Geary's C statistics. All variables exhibited statistically significant spatial patterns. The variable *pc_tree_cv* showed the strongest positive spatial autocorrelation (Moran's I = 0.2337, p = 0.001), followed by *pc_ac* (Moran's I = 0.1747, p = 0.001), while *tree_blt_r* displayed a lower but still significant Moran's I of 0.0181 (p = 0.038). Moran's I and Geary's C values were consistently above 0 for all variables, confirming the presence of positive spatial association. A summary of the results is provided in *Table 2*.

Feature	Moran's I	p-value	Geary's C	p-value
[*pc_ac*] A/C Usage (%)	0.1747	0.001	0.8300	0.001
[*tree_blt_r*] Tree-to-Building Ratio	0.0181	0.038	0.8667	0.007
[*pc_tree_cv*] Tree Coverage (%)	0.2337	0.001	0.7231	0.001
[*pc_nbi0*] Households with 0% UBI (%)	0.1106	0.001	0.8794	0.001
[*pc_met_rf*] Roof - Metal type (%)	0.1081	0.001	0.8974	0.001

Table 2. Summary of Moran's I and Geary's C results.

Prior to model fitting, multicollinearity among covariates was assessed using the Variance Inflation Factor (VIF). All predictors reported VIF values below the critical threshold of 5, indicating no significant multicollinearity. The results are summarized in *Table 3*.

Feature	VIF
const	27.63
log_tree_blt_r	3.86
pc_tree_cv	3.91
pc_nbi0	1.14
pc_met_rf	1.05

Table 3. Summary of VIF results.

Four regression models were estimated to examine the relationship between A/C usage (*log_pc_ac*) and neighborhood-level predictors. *Table 4* presents the estimated coefficients across SDM, SAR, SEM, and OLS models, while *Table 5* summarizes the direct, indirect (spillover), and total effects for the SAR and SDM. Results are as follows:

- The Ordinary Least Squares (OLS) model yielded an R^2 of 0.2573 and showed statistically significant effects for all covariates. *log_tree_blt_r* and *pc_met_rf* had negative coefficients, while *pc_tree_cv* and *pc_nbi0* were positively associated with the dependent variable.
- The Spatial Lag Model (SAR) improved model fit (pseudo R^2 = 0.2817) and confirmed significant spatial lag dependence (*W_log_pc_ac* = 0.3662, $p < 0.001$). The SAR model also showed consistent signs and significance levels for the covariates compared to the OLS model.
- The Spatial Error Model (SEM) provided a comparable pseudo R^2 (0.2567), and the spatial error coefficient (*lambda*) was significant (0.4098, $p < 0.001$), suggesting the presence of spatially correlated omitted variables.
- The Spatial Durbin Model (SDM), which incorporates spatial lags of both the dependent and independent variables, achieved the best overall fit (pseudo R^2 = 0.2931). Significant direct and indirect (spillover) effects were detected.

Features	SDM	SAR	SEM	OLS
const	1.26847	1.23272 ($p < .05$)	2.32266 ($p < .05$)	2.33628 ($p < .05$)
log_tree_blt_r	-0.40929 ($p < .05$)	-0.34374 ($p < .05$)	-0.37742 ($p < .05$)	-0.35322 ($p < .05$)
pc_tree_cv	0.01536 ($p < .05$)	0.01139 ($p < .05$)	0.01211 ($p < .05$)	0.00996 ($p < .05$)
pc_nbi0	0.02071 ($p < .05$)	0.02101 ($p < .05$)	0.02113 ($p < .05$)	0.02266 ($p < .05$)
pc_met_rf	-0.00757 ($p < .05$)	-0.00808 ($p < .05$)	-0.00806 ($p < .05$)	-0.00896 ($p < .05$)
W_log_pc_ac	0.11396	0.36624 ($p < .05$)	-	-
W_log_tree_blt_r	0.97035 ($p < .05$)	-	-	-
W_pc_tree_cv	-0.03713 ($p < .05$)	-	-	-
W_pc_nbi0	0.02183	-	-	-
W_pc_met_rf	-0.00785	-	-	-
lambda	-	-	0.40980 ($p < .05$)	-

Table 4. Estimated coefficients across SDM, SAR, SEM, and OLS models.

Features	Direct	Indirect	Total
SAR			
log_tree_blt_r	-0.3437	-0.1986	-0.5424
pc_tree_cv	0.0114	0.0066	0.0180
pc_nbi0	0.0210	0.0121	0.0331

pc_met_rf	-0.0081	-0.0047	-0.0128
SDM			
log_tree_blt_r	-0.4093	1.0425	0.6332
pc_tree_cv	0.0154	-0.0399	-0.0246
pc_nbi0	0.0207	0.0273	0.0480
pc_met_rf	-0.0076	-0.0098	-0.0174

Table 5. Direct, indirect (spillover), and total effects for the SAR and SDM models.

Table 6 summarizes the model performance metrics. The Durbin model achieved the lowest Akaike Information Criterion (AIC = 1822.60) and the highest log-likelihood (-901.30), indicating the best overall fit. While the SEM model had the lowest Root Mean Squared Error (RMSE = 29.19), its overall fit (AIC and log-likelihood) was inferior to the Durbin model. The SAR and OLS models followed in performance, with the OLS model being the least performant across all metrics. Figure 22 illustrates the predictions for each of the four spatial regression models.

Model	AIC	Log-Likelihood	RMSE
Durbin (SDM)	1822.60	-901.30	28.21
SAR (Lag)	1826.61	-907.31	28.21
SEM (Error)	1830.18	-910.09	29.19
OLS	1841.36	-915.68	29.30

Table 6. Model performance metrics across all models (i.e. SDM, SAR, SEM, and OLS) based on AIC, log-likelihood and RMSE.

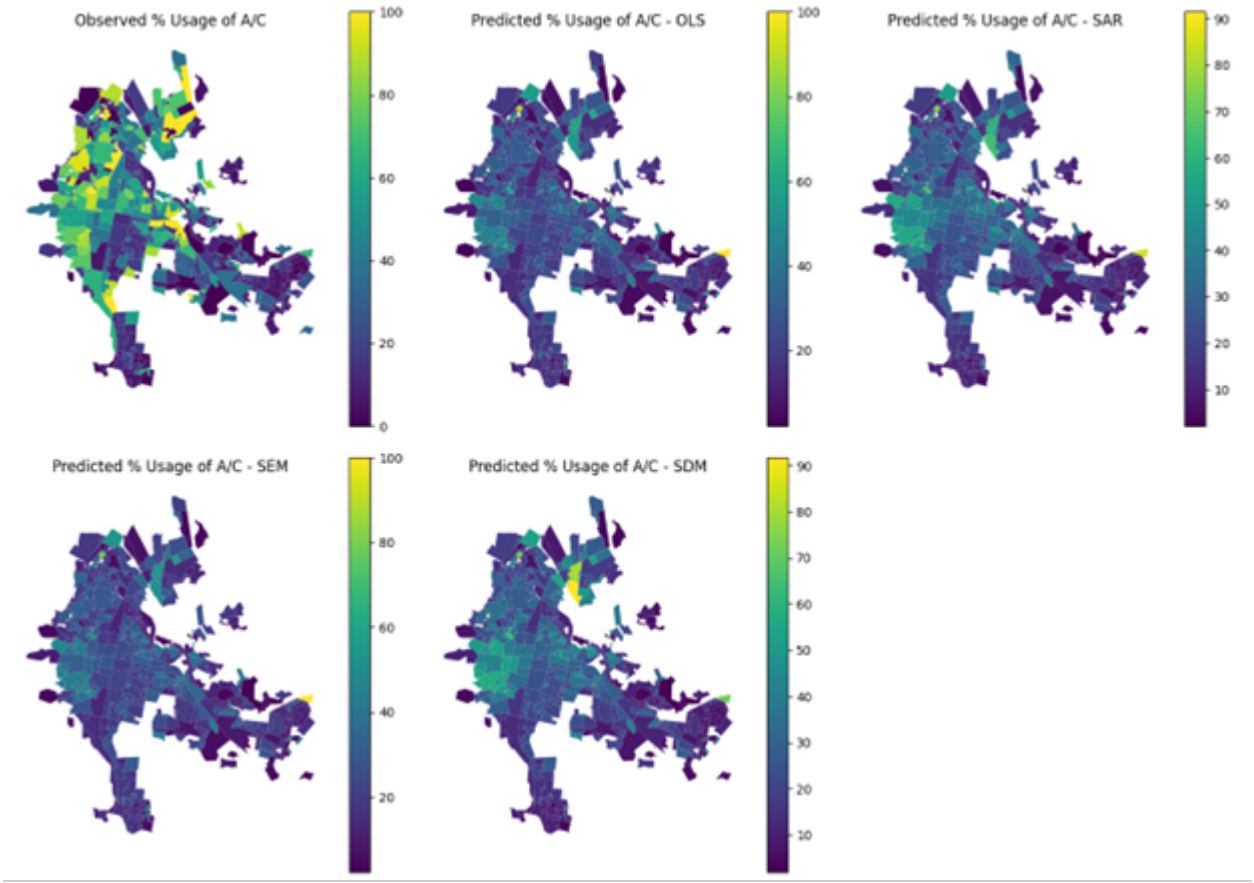

Figure 22. Observed and predicted A/C usage for each of the four spatial regression models (i.e. SDM, SAR, SEM, and OLS) across neighborhoods of San Pedro Sula.

Although Gaussian regression models yielded satisfactory results, an alternative approach based on count data models was explored, which may be more appropriate given the nature of the response variable (i.e. in %). Specifically, the A/C count as a binomial outcome was modelled, where the number of trials in each neighborhood corresponds to the total number of households, and the number of "successes" represents households with A/C use. The binomial model is well suited for this type of proportion data, as it directly models the probability of success (i.e., the probability that a household has A/C) within a fixed number of trials. In order to take into account the spatial autocorrelation present in the data, both the binomial Leroux and BYM spatial models have been considered. These models were fitted using the *CARBayes* (Lee, 2013) package in *R*, which implements a fully Bayesian framework for spatial generalized linear models. Parameter estimation in CARBayes was performed via MCMC sampling, allowing for the computation of posterior distributions and credible intervals for all model parameters.

In Table 7, the parameter estimates for these two models are presented. The first column lists each parameter, while the second and third columns show the posterior mean along with the 95% credible interval (in parentheses) for the Leroux and BYM spatial binomial models, respectively. These intervals, as defined within a Bayesian approach, indicate the uncertainty around each estimate. If the credible interval contains zero, it suggests that the effect may not be statistically significant at the 95% level; conversely, intervals that do not include zero indicate strong evidence of an effect in the direction of the estimate.

Parameter	Mean (CI) Leroux	Mean (CI) BYM
(Intercept)	-1.4839 (-1.9781; -0.9326)	-1.6236 (-2.1980; -0.9981)
log_tree_blt_r	-0.2764 (-0.4982; -0.0335)	-0.3172 (-0.4460; -0.1379)
pc_tree_cv	0.0056 (-0.0039; 0.0146)	0.0091 (0.0020; 0.0143)
pc_nbi0	0.0318 (0.0259; 0.0374)	0.0302 (0.0254; 0.0349)
pc_met_rf	-0.0171 (-0.0208; -0.0115)	-0.0148 (-0.0194; -0.0111)
tau2	8.0114 (3.8987; 17.4431)	21.4638 (14.5091; 31.8203)
rho	0.0862 (0.0253; 0.2294)	-
sigma2	-	1.2573 (0.9276; 1.6052)
WAIC	3495	3516
RMSE	0.7053	0.7176

Table 7. Results of the spatial binomial models.

The spatial Leroux binomial model demonstrates slightly superior performance compared to the spatial BYM binomial model, as evidenced by its lower WAIC (3495 vs. 3516) and RMSE (0.7053 vs. 0.7176). In addition, when comparing both spatial binomial models to the Gaussian models, the improvement in predictive performance is even more pronounced. These results suggest that the Leroux model provides a better balance between model fit and complexity (as indicated by WAIC), and more accurate predictions (as indicated by RMSE). Furthermore, *Figure 23* presents the maps of the observed and predicted A/C usage percentages across neighborhoods, estimated using both models. The high similarity between the observed and predicted maps indicates that both spatial binomial models achieve strong predictive accuracy.

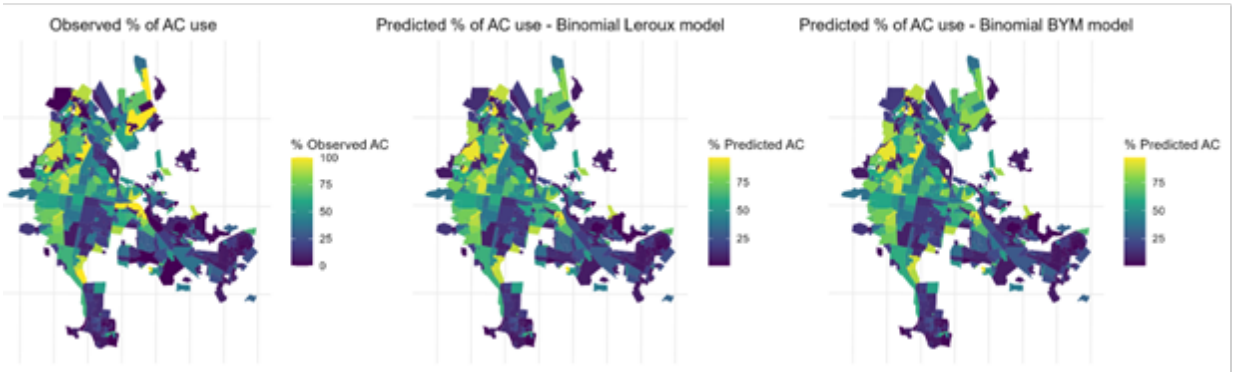

Figure 23. Observed and predicted A/C usage percentages across neighborhoods, estimated using both models (i.e. Binomial Lreoux and Binomial BYM models).

In terms of parameter estimates, both models identify similar relationships between predictors and the probability of A/C use. For example, the variable *log_tree_blt_r* (log-transformed tree to building ratio) is statistically significant since zero is not contained in the 95% credible interval and is negatively associated with A/C use in both models, suggesting that areas with denser vegetation tend to have fewer households with A/C use. Conversely, variables such as *pc_nbi0* (percentage of households with no basic needs unsatisfactorily attended), also statistically significant, show a consistent positive effect. The Leroux model also estimates a relatively low spatial autocorrelation parameter, rho, indicating a small but statistically significant presence of spatial autocorrelation being captured by this model. Overall, the results support the use of the spatial binomial Leroux model as the most effective approach among those tested, offering both improved predictive accuracy and interpretable spatial effects. Since the Leroux model demonstrated the best overall performance, a specific focus was given to this model for a more detailed interpretation of the covariate effects. Specifically, the marginal effects on the predicted probability of A/C use were analyzed, given a one-unit increase in each covariate, while holding other variables constant. The results are summarized in *Figure 24*. The points represent the mean marginal effect for each covariate, and the horizontal lines indicate the 95% credible intervals. Interpretation of this marginal effect is given in the Discussion section.

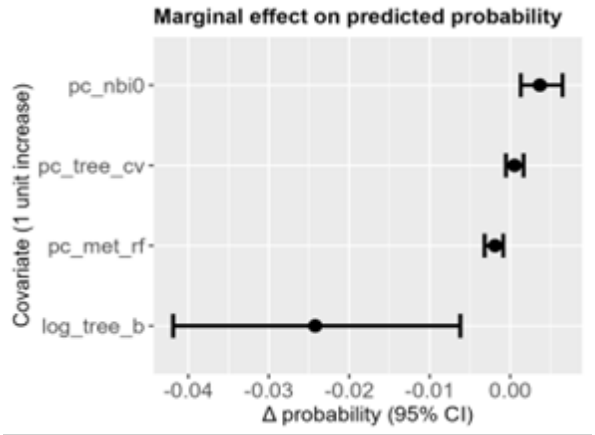

Figure 24. Marginal effects on the predicted probability of A/C usage.

As illustrated in *Figure 25*, bivariate LISA analysis reveals the spatial association between local *A/C usage* and neighboring tree cover (i.e. *tree canopy coverage*), identifying distinct clusters across the study area. Statistically significant clusters ($p < .05$) indicate neighborhoods where A/C demand is spatially linked to tree coverage in adjacent areas. A

total of 33 neighborhoods exhibited *High-High* (HH) clustering, characterized by high local A/C usage and high surrounding tree cover. 104 neighborhoods fell into the *Low-Low* (LL) cluster, with both low local A/C usage and low tree coverage in neighboring areas. Also, 113 neighborhoods were identified as *High-Low* (HL), signifying areas with high local A/C usage and low greening in surrounding areas. Last, 93 neighborhoods were classified as *Low-High* (LH), reflecting areas with low local A/C usage and high tree presence in surrounding areas. The remaining 244 neighborhoods did not display statistically significant spatial clustering, suggesting no clear spatial association between A/C usage and neighboring tree cover in those areas.

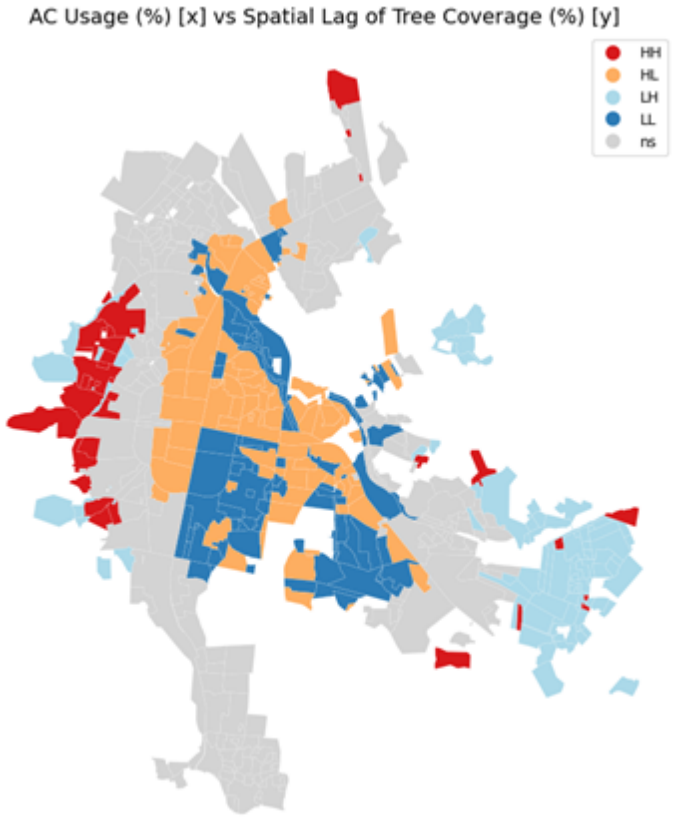

Figure 25. Bivariate LISA analysis of local A/C usage (%) and the tree coverage (%).

As illustrated in *Figure 26*, bivariate LISA analysis between local *A/C usage* and the *tree-to-building ratio* highlights the spatial association between cooling demand and neighboring greening intensity relative to built form. Statistically significant clusters ($p < .05$) reveal distinct neighborhood patterns. Specifically, 10 neighborhoods exhibited *High-High* (HH) clustering, where elevated A/C usage coincides with high surrounding tree-to-building ratios. In contrast, 91 neighborhoods fell into the *Low-Low* (LL) cluster, reflecting areas with both low A/C usage and low nearby tree-to-building ratios. A total of 70

neighborhoods were identified as *High-Low* (HL), characterized by high local A/C usage despite low neighboring tree-to-building ratios, while 27 neighborhoods were classified as *Low-High* (LH), with low local A/C demand and high greening relative to building density in adjacent areas. The majority of neighborhoods (n = 389) did not exhibit statistically significant clustering, indicating limited spatial dependence between A/C usage and tree-to-building ratios across much of the study area.

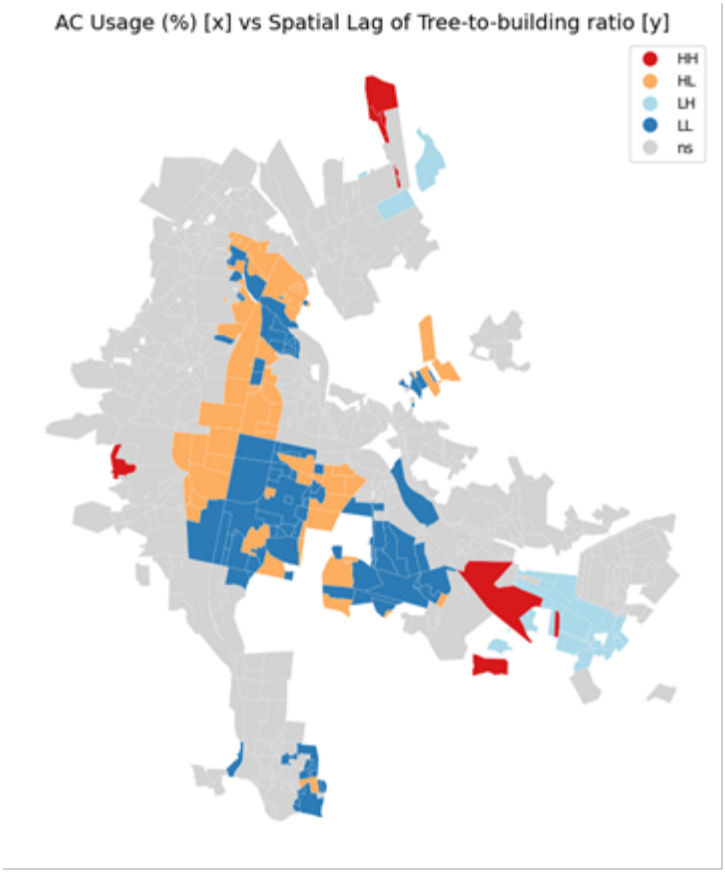

Figure 26. Bivariate LISA analysis of local A/C usage (%) and the tree-to-building ratio.

4. Discussion

This research situates the analysis in Honduras, where A/C access and use are strongly shaped by socio-economic inequality. In the Honduran context, remote sensing studies have begun to document the impacts of urbanization on urban greenness in Tegucigalpa (Reyes-Avila & Baxter, 2024). However, to the author's knowledge, no research has yet examined how tree canopy directly influences cooling demand and A/C usage in this tropical, low-income setting. Although urban greenery in city environments

are linked to multiple social and environmental benefits (i.e., biodiversity promotion, stormwater attenuation, air quality improvement, property value uplift, street attractiveness for retail, urban safety and liveliness) (Trees & Design Action Group (TDAG), 2012; S. Yang et al., 2025), the present study addresses a specific gap: understanding the role of trees in reducing building energy cooling demand.

4.1 Effect of trees and covariates

Across all Gaussian regression models (i.e. OLS, spatial lag, spatial error, and spatial Durbin):

- The *pc_nbi0*, representing the percentage of homes with zero unsatisfied basic needs, consistently emerges as the variable with the strongest effect on neighborhood-level A/C usage, except in count data models, where *log_tree_blt_r* (log-transformed tree-to-building ratio) has the largest impact among the environmental variables. Its coefficient of *pc_nbi0* is positive and highly significant in every model, indicating that neighborhoods where more households have all basic needs are met tend to exhibit higher A/C usage. Compared to other factors, *pc_nbi0* stands out as the dominant socioeconomic determinant, highlighting that higher household well-being is a key driver of A/C usage at the neighborhood scale. These findings align with previous research suggesting that energy demand for air conditioning is projected to increase rapidly over the whole 2000–2100 period, *mostly driven by income growth* (Isaac & van Vuuren, 2009).
- The coefficient for metal roofs (*pc_met_rf)* is consistently negative, likely indicating that neighborhoods with a higher prevalence of metal-roofed houses tend to have lower A/C usage. In light of studies on indoor overheating risk in buildings, this seemingly counterintuitive result likely reflects socioeconomic patterns. Results indicate that poorer neighborhoods are more likely to have metal roofs, but residents in these areas may have limited access to or affordability for A/C, resulting in lower observed usage. While most studies on overheating risk associate metal roofs, particularly when uninsulated, with higher indoor temperatures and increased cooling demand (Fosas et al., 2018; Hashemi, 2017), models' results suggest that *financial constraints may outweigh or override the physical drivers of A/C adoption* (i.e., even if a metal roof makes indoors hotter, people might not install A/C if they can't afford it). Nonetheless, this interpretation remains a hypothesis, and future research with in-situ measurements is needed to validate whether socioeconomic constraints indeed outweigh the physical drivers of A/C adoption in neighborhoods with metal roofs.

- For the tree-to-building ratio (*log_tree_blt_r*), the models consistently show that a 1-unit increase in the log of tree-to-building ratio leads to a substantial reduction in A/C prevalence. Across the OLS, SAR, SEM, and SDM models, the direct effect ranges from -34.4% to -40.9%, meaning households in neighborhoods with more trees relative to buildings are significantly less likely to adopt A/C. In practical terms, increasing the tree-to-building ratio from 1:1 to 2:1, equivalent to doubling tree area relative to buildings, translates into a 21-25% reduction in A/C prevalence. This practical example highlights that even *modest improvements in tree presence at the neighborhood scale can yield sizable reductions in cooling demand in San Pedro Sula*, which in turn may lessen the need to expand electrical grid infrastructure to satisfy peak cooling loads. Results of this study are consistent with previous simulation studies, which show cooling energy reductions of up to 40% when vegetative cover is increased by 30% (Akbari & Taha, 1992).

- Although Figure 16 (correlogram) shows a negative association between *pc_tree_cv* and A/C usage, when fitting the spatial regression models an apparent paradox emerges from the results: increasing *tree coverage* (*pc_tree_cv*) increases A/C usage, whereas increasing the *tree-to-building ratio* (*log_tree_blt_r*) lowers A/C usage. This contrast arises because the two features, though both related to tree presence, seem to capture different urban realities. The percentage of tree cover (*pc_tree_cv*) is often high in low-density, high-income neighborhoods with large lots, private gardens, or adjacent parks. In such settings, households typically occupy larger homes and possess greater purchasing power, making A/C adoption more likely, even when greenery is abundant. In these cases, trees seem to contribute to overall neighborhood coverage but provide limited direct shading to the buildings themselves. By contrast, the tree-to-building ratio (*log_tree_blt_r*) seems to reflect the balance between vegetated and built surfaces, likely capturing the extent to which trees provide shading and evapotranspiration relative to building mass. In dense neighborhoods with compact housing, even some tree presence (e.g., street trees, trees in courtyards) can provide meaningful cooling benefits. The *tree coverage* appears to act as a proxy for income, while the *tree-to-building ratio* more directly reflects trees' capacity to offset cooling needs. This distinction is evident in the LISA results (*Figure 25* and *Figure 26*). For insgtance, numerous neighborhoods were classified as HH (high A/C usage with high surrounding *tree coverage*) when using *pc_tree_cv*; however, only a handful appeared as HH (high A/C usage with high surrounding *tree-to-building ratio*) when using *tree_blt_r*. In other words, areas with high A/C usage and high greenness under the *tree coverage* indicator do not necessarily remain in the same category when greenness is normalized by building footprint (i.e. *tree-to-building ratio*).

Across count data models, it is worth noting interpreting the results of the Leroux model, the most performative one:

- The *pc_nbi0* (percentage of households with no unattended basic needs) shows the largest and most significant positive effect, indicating that households in neighborhoods with better socioeconomic conditions are substantially more likely to use A/C more. The coefficient of *pc_tree_cv* (log-transformed tree coverage) also exhibits a small but significant positive effect, while *pc_met_rf* displays a small yet significant negative effect on A/C use probability.

- The *log_tree_blt_r* (log-transformed tree-to-building ratio) shows a statistically significant negative effect, with its 95% credible interval also excluding zero. This indicates that households in neighborhoods with higher tree-to-building ratios are less likely to use A/C. However, the credible interval is relatively wide, suggesting substantial uncertainty about the exact magnitude of this effect. While it can be confidently stated the direction of the association (negative), the variability implies that the strength of the relationship may differ across neighborhoods. In particular, as shown in *Figure 24*, the marginal effects indicate that *log_tree_blt_r* (log-transformed tree-to-building ratio) has the largest impact among the environmental variables, with a one-unit increase associated with a decrease of about 0.0242 (−0.0419; −0.0062) in the predicted probability of A/C use of each household. In contrast, *pc_nbi0* (percentage of households with no unmet basic needs) shows a positive association, where a one-unit increase leads to an increase of approximately 0.0037 (0.0013; 0.0065) in the predicted probability. The effects of *pc_tree_cv* (percentage of tree coverage) and *pc_met_rf* (percentage of metallic roofs) are smaller in magnitude, with changes of +0.0005 (−0.0005; 0.0017) and −0.0019 (−0.0032; −0.0009), respectively.

4.2 Neighborhood patterns

In terms of the effect of neighbor's trees on local A/C usage, as illustrated in *Figure 25* and *Figure 26*, The bivariate LISA results reveal a complex relationship between A/C usage and trees presence in neighborhoods (i.e. *tree-to-building ratio*, *tree canopy coverage*):

- The *HL cluster* (orange zones), where A/C usage is high, but neighboring areas are low in *tree coverage* or *tree-to-building ratio*, emerges as particularly concerning. These neighborhoods appear to be thermally isolated, lacking access to the cooling benefits of nearby vegetation. From a spatial policy lens, they represent high-priority zones for targeted nature-based interventions (e.g. tree planting), and spatial regression models corroborate it. For instance, the Spatial Autoregressive

Model (SAR) revealed a negative and significant indirect effect (-0.1986) of the *tree-to-building ratio* (*log_tree_blt_r*) on A/C usage, and the Spatial Durbin Model (SDM) and the Spatial Autoregressive Model (SAR) a negative and significant indirect effect (-0.0399) of *tree coverage* (*pc_tree_cv*) on A/C usage. This implies that greening in surrounding neighborhoods can reduce local demand for A/C usage (beneficial spatial spillover effects). In other words, residents may indirectly benefit from shade, evapotranspiration, and cooler airflows generated by trees in nearby areas, even if their own neighborhood has limited vegetation. Neighborhoods within the HL cluster (where tree presence is scarce), including the City Center of San Pedro Sula with a *tree coverage* of 2.77% and a *tree-to-building ratio* of 1:11, may benefit from urban greening interventions.

- The *LL clusters* (blue zones) correspond to neighborhoods characterized by both low A/C usage and limited surrounding *tree coverage* and *tree-to-building ratio*, conditions that suggest potential environmental vulnerability due to insufficient outdoor and indoor cooling. This dual exposure highlights a critical need for passive cooling strategies, such as increased urban greenery. However, this assumption should be proven through empirical measurements (not within the objectives or scope of this study), as elevated outdoor temperatures in these areas may be contributing to indoor overheating risk. Unlike the HH cluster, where *tree coverage* and the *tree-to-building ratio* identify different neighborhoods, the LL clusters are largely consistent across both indicators. This suggests that, at the lower end of A/C usage and tree greenness, both effectively highlight deprived neighborhoods surrounded by areas lacking trees, providing a clear signal for urban cooling interventions.

- The *LH clusters* (light blue) may represent “green halo” neighborhoods, characterized by low A/C usage alongside high levels of *tree coverage* and *tree-to-building ratio* in surrounding areas. Although this spatial pattern may suggest that vegetation in adjacent neighborhoods contributes to localized passive cooling due to trees (supporting the hypothesis that urban greening offers indirect thermal benefits), the effect of *pc_nbi0* on lower A/C usage also suggests that it may not necessarily result from diminished cooling needs driven by tree presence; rather, it could reflect urban inequalities, such as limited access to A/C in lower-income areas.

- The *HH clusters* (red), with high A/C demand, and high neighboring *tree coverage* and *tree-to-building ratio*, likely represent wealthy, low-density neighborhoods where cooling behaviors are decoupled from environmental need and instead reflect lifestyle or cultural preferences.

4.3 Limitations and future research work

This study has several limitations that should be acknowledged. Because indoor temperature data collection was beyond the scope of this study, it was not possible to directly link outdoor tree cover with household indoor thermal comfort or energy use. Similarly, the absence of building level information (e.g., density, form, available open space) constrains the accuracy of identifying neighborhood-specific drivers of low tree cover, however, this also falls outside the scope of this study. The AI segmentation model, while very useful, still faces accuracy constraints due to limited labelled training data (i.e. only 19 aerial images were used for training), which may affect the reliability of tree canopy detection. Finally, urban heat island (UHI) effect was not directly measured or integrated, reducing the capacity to validate neighborhood level thermal risks, also out of scope of this study. Building on these limitations, future studies should prioritize in situ monitoring or building energy simulations to establish more direct links between greenery, indoor thermal comfort, and A/C demand. Research should also investigate the spatial barriers behind low tree coverage in high A/C usage areas, including constraints such as high density, impervious surfaces, or limited available land. Detailed spatial diagnostics of buildable land, parking lots, and other impervious areas could help identify opportunities for intervention. Future work should also expand the scope of solutions to include nature-based and complementary strategies (e.g., green roofs, facades, reflective surfaces, targeted tree planting) that are tailored to constraints on neighborhoods. Moreover, incorporating UHI data from satellite imagery could strengthen the prioritization of interventions in vulnerable areas. Finally, fine-tuning AI segmentation models with additional labelled data would improve canopy detection accuracy and enhance the robustness of future analyses.

5. Conclusions

For San Pedro Sula, Honduras, this study integrates AI-based tree mapping, census data, and advanced spatial regression models to identify neighborhoods with elevated A/C usage. Higher A/C prevalence is partly linked to limited tree presence (i.e. lower *tree-to-building ratio*) alongside built environment and socioeconomic factors, such as roof type (i.e. metal) and unmet basic needs.

5.1 Main findings

The key findings of this study are as follows:

- Approximately 45% of the city of San Pedro Sula is covered by trees; however, *tree coverage* varies widely across neighborhoods, ranging from less than 1% in high-density neighborhoods up to nearly 98% in low-density neighborhoods, and a median *tree coverage* of 29.6%.
- Across neighborhoods the median *tree-to-building ratio* is 1.49:1, which highlights both the variability (i.e. between tree presence and building footprint) and the potential for targeted urban greening interventions in "vulnerable" neighborhoods.
- Overall, 26.1% of households report having A/C, though prevalence varies across neighborhoods, from areas with no A/C-equipped households to neighborhoods where all households have A/C, reflecting underlying socioeconomic disparities.
- Spatial regression results indicate that increasing tree canopy area relative to building area significantly reduces *A/C usage*: a unit increase in the *tree-to-building ratio* (log scale) corresponds to a 34–41% decrease in A/C prevalence. In practical terms, doubling tree cover relative to building footprint (from 1:1 to 2:1) is associated with a 21–25% reduction in A/C usage, and tripling the ratio (from 1:1 to 3:1) corresponds to roughly 38–45% lower A/C prevalence, highlighting the potential for measurable energy savings through targeted urban greening with trees.
- In addition, the spatial count data models indicate that a one unit increase in the *tree-to-building ratio* (log scale) is associated with an approximate 2.4% reduction in the probability that a household uses A/C. The 95% credible interval ranges from a reduction of 0.6 to 4.2 percentage points, providing strong evidence that the association is negative.
- The analysis further demonstrates that the *tree coverage* (%) indicator captures greenness in absolute surface terms, which often coincides with wealthier, lower-density areas where A/C usage is high despite greenery.
- By contrast, the *tree-to-building ratio* provides a normalized measure of greenness relative to built form, making it more sensitive to shading and

microclimatic benefits per building, and therefore showing stronger alignment with lower *A/C usage*.

- Spatial analysis emphasizes that urban greening is not just about adding trees, but also about where and how they are added. Combined findings from spatial regression and LISA analyses indicate that nature-based strategies like planting trees must be geographically targeted, since uniform or isolated tree planting risks benefiting already "green" or well-resourced neighborhoods while leaving heat-vulnerable areas without relief. Effective interventions should consider localized needs and systemic spatial patterns, prioritizing neighborhoods with limited tree cover, high A/C usage (or high indoor temperatures, high indoor overheating degrees), and greater social vulnerability.

5.2 Practical application for humanitarian work and recommendations

From a humanitarian perspective, the findings of this study provide a data-driven approach to identify priority areas for interventions aimed at creating (indoor or outdoor) heat resilience. Practical applications of this approach include informing the placement of tree-planting campaigns and other nature-based solutions (e.g. green roofs, reflective surfaces, and street shading) in heat-vulnerable, A/C-reliant areas to maximize both social and environmental benefits. By leveraging AI-based tree mapping, census data, and spatial regression models, planners and NGOs can pinpoint neighborhoods most in need, ensuring resources on areas with the highest heat exposure and energy burdens, to improve thermal comfort, reduce A/C reliance, and strengthen urban resilience, particularly for the most vulnerable populations. Humanitarian actors can complement this data-driven approach with community engagement, local capacity building, and monitoring programs, combining spatial diagnostics with in-home temperature measurements to cross-validate outcomes. Based on these findings, the study suggests the following recommendations:

- NGOs and humanitarian actors should co-develop interventions with local residents (e.g. through the "Patronato" of neighbors of each neighborhood), ensuring cultural appropriateness and building local ownership of green infrastructure projects. *Note based on findings: in this study, the HL (high local A/C usage, low spatially lagged tree coverage) cluster from LISA findings identify thermally isolated neighborhoods where participatory tree-planting can reduce need of using A/C.*

- Position urban heat resilience as part of humanitarian disaster risk reduction frameworks, linking it to early warning systems, public health preparedness, and climate migration strategies. *Note based on findings: in this study, the LL (low local A/C usage, low spatially lagged tree coverage) cluster, with low A/C access and low greenery,*

illustrates how heat exposure (i.e. low or none A/C usage) intersects with environmental vulnerability (i.e. low tree coverage).

- Paying attention to marginalized groups (i.e. informal settlement residents, older adults, and women-headed households) is crucial, by tailoring cooling measures (e.g., tree-shaded communal areas) to their specific vulnerabilities. *Note based on findings: in this study, evidence that households with metal roofs use less A/C due to affordability rather than comfort signals the need to target low-income, infrastructurally deprived groups with passive cooling solutions.*

References

Akbari, H., & Taha, H. (1992). The impact of trees and white surfaces on residential heating and cooling energy use in four Canadian cities. *Energy*, *17*(2), 141–149. https://doi.org/10.1016/0360-5442(92)90063-6

Al-Sallal, K. A., & Al-Rais, L. (2011). *Mitigating Heat Gain Using Greenery of an Eco-House in Abu Dhabi*.

Angel, S., Derr, M., Malur, A., Mejía, J., Nuka, P., Perlin, M., & Sahai, S. (2004). *Rapid Urbanization in Tegucigalpa , Honduras*. *February*.

Anilturk, O., Lumanauw, E., Bird, J., Olloniego, J., Laird, D., Fernandez, J. C., & Killough, Q. (2023). Automatic defect classification (ADC) solution using data-centric artificial intelligence (AI) for outgoing quality inspections in the semiconductor industry. *Https://Doi.Org/10.1117/12.2658434*, *12496*, 830–836. https://doi.org/10.1117/12.2658434

Anselin, L. (1988). *Spatial Econometrics: Methods and Models*. *4*. https://doi.org/10.1007/978-94-015-7799-1

Anselin, L. (1995). Local Indicators of Spatial Association—LISA. *Geographical Analysis*, *27*(2), 93–115. https://doi.org/10.1111/J.1538-4632.1995.TB00338.X

Besag, J., York, J., & Mollié, A. (1991). Bayesian image restoration, with two applications in spatial statistics. *Annals of the Institute of Statistical Mathematics*, *43*(1), 1–20. https://doi.org/10.1007/BF00116466

Boeing, G. (2025). Modeling and Analyzing Urban Networks and Amenities With OSMnx. *Geographical Analysis*. https://doi.org/10.1111/GEAN.70009

Bosch, M. (2020). DetecTree: Tree detection from aerial imagery in Python. *Journal of Open Source Software*, *5*(50), 2172. https://doi.org/10.21105/JOSS.02172

Carías, A. (2013). Variabilidad climática en las ciudades urbanas de Tegucigalpa y Comayagüela, Francisco Morazán, Honduras en el 1975 - 2011. *Revista Ciencias Espaciales*, *6*(2 Otoño), 34–47. https://doi.org/10.5377/ce.v6i2.2466

Chagolla, M. A., Alvarez, G., Simá, E., Tovar, R., & Huelsz, G. (2013). Effect of Tree Shading on the Thermal Load of a House in a Warm Climate Zone in Mexico. *ASME International Mechanical Engineering Congress and Exposition, Proceedings (IMECE)*, *7*(PARTS A, B, C, D), 761–768. https://doi.org/10.1115/IMECE2012-87918

Clark, J. (2025). *Pillow (PIL Fork) 11.3.0 documentation*. https://pillow.readthedocs.io/en/stable/index.html

Donovan, G. H., & Butry, D. T. (2009). The value of shade: Estimating the effect of urban trees on summertime electricity use. *Energy and Buildings*, *41*(6), 662–668. https://doi.org/10.1016/J.ENBUILD.2009.01.002

Fosas, D., Coley, D. A., Natarajan, S., Herrera, M., Fosas de Pando, M., & Ramallo-Gonzalez, A. (2018). Mitigation versus adaptation: Does insulating dwellings increase overheating risk? *Building and Environment*, *143*, 740–759. https://doi.org/10.1016/J.BUILDENV.2018.07.033

Gamero-Salinas, J. C., Monge-Barrio, A., & Sanchez-Ostiz, A. (2020). A thermal comfort assessment in a rehabilitated residential building of the city center of Tegucigalpa, Honduras. In I. Lombillo, H. Blanco, & Y. Boffill (Eds.), *REHABEND 2020 - 8h Euro-American Congress: Construction Pathology, Rehabilitation Technology and Heritage Management* (pp. 1849–1856). University of Cantabria – Building Technology R&D Group.

Gamero-Salinas, J. C., Monge-Barrio, A., & Sánchez-Ostiz, A. (2020). Overheating risk assessment of different dwellings during the hottest season of a warm tropical climate. *Building and Environment*, *171*, 106664. https://doi.org/https://doi.org/10.1016/j.buildenv.2020.106664

Gamero-Salinas, J., & López-Fidalgo, J. (2024). *Response Surface Methodology coupled with desirability functions for multi-objective optimization: minimizing indoor overheating hours and maximizing useful daylight illuminance*. https://arxiv.org/abs/2409.09093v1

Gamero-Salinas, J., Monge-Barrio, A., Kishnani, N., López-Fidalgo, J., & Sánchez-Ostiz, A. (2021). Passive cooling design strategies as adaptation measures for lowering the indoor overheating risk in tropical climates. *Energy and Buildings*, *252*, 111417. https://doi.org/10.1016/J.ENBUILD.2021.111417

Geary, R. C. (1954). The Contiguity Ratio and Statistical Mapping. *The Incorporated Statistician*, *5*(3), 115. https://doi.org/10.2307/2986645

Getis, A., & Aldstadt, J. (2004). Constructing the Spatial Weights Matrix Using a Local Statistic. *Geographical Analysis*, *36*(2), 90–104. https://doi.org/10.1111/J.1538-4632.2004.TB01127.X

Gillies, S. (2013). *Rasterio: Geospatial raster I/O for Python programmers*.

Google. (2025). *Google Colab*. https://colab.research.google.com/

Haklay, M., & Weber, P. (2008). OpenStreet map: User-generated street maps. *IEEE Pervasive Computing*, *7*(4), 12–18. https://doi.org/10.1109/MPRV.2008.80

Hamdan, M., Badr, Z., Bjork, J., Saxe, R., Malensek, F., Miller, C., Shah, R., Han, S., & Mohammad-Rahimi, H. (2023). Detection of dental restorations using no-code artificial intelligence. *Journal of Dentistry*, *139*, 104768. https://doi.org/10.1016/J.JDENT.2023.104768

Hashemi, A. (2017). Effects of thermal insulation on thermal comfort in low-income tropical housing. *Energy Procedia*, *134*, 815–824. https://doi.org/10.1016/J.EGYPRO.2017.09.535

Hwang, H. W., Eric Wiseman, P., Thomas, V. A., Hoi, W., & Eric, P. (2016). Simulation of Shade Tree Effects on Residential Energy Consumption in Four U.S. Cities. *Cities and the Environment (CATE)*, *9*(1). https://doi.org/10.15365/1932-7048.1202

INE. (2025). *Sitio web oficial - Instituto Nacional de Estadística de Honduras(INE)*. https://ine.gob.hn/v4/

Isaac, M., & van Vuuren, D. P. (2009). Modeling global residential sector energy demand for heating and air conditioning in the context of climate change. *Energy Policy*, *37*(2), 507–521. https://doi.org/10.1016/J.ENPOL.2008.09.051

Ko, Y. (2018). Trees and vegetation for residential energy conservation: A critical review for evidence-based urban greening in North America. *Urban Forestry & Urban Greening*, *34*, 318–335. https://doi.org/10.1016/J.UFUG.2018.07.021

Ko, Y., Lee, J. H., McPherson, E. G., & Roman, L. A. (2015). Long-term monitoring of Sacramento Shade program trees: Tree survival, growth and energy-saving performance. *Landscape and Urban Planning*, *143*, 183–191. https://doi.org/10.1016/J.LANDURBPLAN.2015.07.017

Laband, D. N., & Sophocleus, J. P. (2009). An Experimental Analysis of the Impact of Tree Shade on Electricity Consumption. *Arboriculture & Urban Forestry (AUF)*, *35*(4), 197–202. https://doi.org/10.48044/JAUF.2009.033

LandingAI. (2025). *LandingLens: Deep-Learning Computer Vision Software Platform*. https://landing.ai/landinglens

Lee, D. (2013). CARBayes: An R Package for Bayesian Spatial Modeling with Conditional Autoregressive Priors. *Journal of Statistical Software*, *55*(13), 1–24. https://doi.org/10.18637/JSS.V055.I13

Leroux, B. G., Lei, X., & Breslow, N. (2000). *Estimation of Disease Rates in Small Areas: A new Mixed Model for Spatial Dependence*. 179–191. https://doi.org/10.1007/978-1-4612-1284-3_4

LeSage, J., & Pace, R. K. (2009). *Introduction to Spatial Econometrics*. https://doi.org/10.1201/9781420064254

Mahajan, S. (2024). greenR: An open-source framework for quantifying urban greenness. *Ecological Indicators*, *163*, 112108. https://doi.org/10.1016/J.ECOLIND.2024.112108

McPherson, E. G., & Rowntree, R. A. (1993). Energy conservation potential of urban tree planting. *Journal of Arboriculture. 19: 321-331*, *19*(6), 321–331. https://research.fs.usda.gov/treesearch/61734

McPherson, E. G., & Simpson, J. R. (2003). Potential energy savings in buildings by an urban tree planting programme in California. *Urban Forestry & Urban Greening*, *2*(2), 73–86. https://doi.org/10.1078/1618-8667-00025

Mejía, E. J. (2018). *Comportamiento y Variación Decadal de la Temperatura en la Ciudad de Tegucigalpa en el Periodo de 1980 - 2009*. https://ihcit.unah.edu.hn/dmsdocument/5362-variacion-decadal-de-temperatura-en-tegucigalpa-pdf

Morakinyo, T. E., Balogun, A. A., & Adegun, O. B. (2013). Comparing the effect of trees on thermal conditions of two typical urban buildings. *Urban Climate*, *3*, 76–93. https://doi.org/10.1016/J.UCLIM.2013.04.002

Morakinyo, T. E., Kong, L., Lau, K. K. L., Yuan, C., & Ng, E. (2017). A study on the impact of shadow-cast and tree species on in-canyon and neighborhood's thermal comfort. *Building and Environment*, *115*, 1–17. https://doi.org/10.1016/J.BUILDENV.2017.01.005

Moran, P. A. P. (1948). The interpretation of statistical maps. *Journal of the Royal Statistical Society. Series B (Methodological)*, *10*(2), 243–251.

Onishi, A., Cao, X., Ito, T., Shi, F., & Imura, H. (2010). Evaluating the potential for urban heat-island mitigation by greening parking lots. *Urban Forestry and Urban Greening*, *9*(4), 323–332. https://doi.org/10.1016/J.UFUG.2010.06.002

Pandit, R., & Laband, D. N. (2010). Energy savings from tree shade. *Ecological Economics*, *69*(6), 1324–1329. https://doi.org/10.1016/J.ECOLECON.2010.01.009

Pedregosa, F., Varoquaux, G., Gramfort, A., Michel V. and Thirion, B., Grisel, O., Blondel, M., Prettenhofer P. and Weiss, R., Dubourg, V., Vanderplas, J., Passos, A., Cournapeau,

D., Brucher, M., Perrot, M., & Duchesnay, E. (2011). Scikit-learn: Machine Learning in Python. *Journal of Machine Learning Research*, *12*, 2825–2830.

Ravi, N., Gabeur, V., Hu, Y. T., Hu, R., Ryali, C., Ma, T., Khedr, H., Rädle, R., Rolland, C., Gustafson, L., Mintun, E., Pan, J., Alwala, K. V., Carion, N., Wu, C. Y., Girshick, R., Dollár, P., & Feichtenhofer, C. (2024). SAM 2: Segment Anything in Images and Videos. *13th International Conference on Learning Representations, ICLR 2025*, 41175–41218. https://arxiv.org/pdf/2408.00714

Reyes-Avila, A. D., & Baxter, R. A. (2024). Assessment of urbanization impacts in Tegucigalpa urban greenness via normalized difference vegetation index. *Trees, Forests and People*, *18*, 100680. https://doi.org/10.1016/J.TFP.2024.100680

Rey, S. J., & Anselin, L. (2007). PySAL: A Python library of spatial analytical methods. *Review of Regional Studies*, *37*(1), 5–27. https://asu.elsevierpure.com/en/publications/pysal-a-python-library-of-spatial-analytical-methods

Rouse, J. W. , Jr., Haas, R. H., Schell, J. A., & Deering, D. W. (1974). Monitoring vegetation systems in the Great Plains with ERTS. *NASA. Goddard Space Flight Center 3d ERTS-1 Symp., Vol. 1, Sect. A*.

SINIT. (2025). *Visor SINIT (Sistema Nacional de Información Territorial de Honduras)*. https://sinit.hn/visor-del-sinit/

Trees & Design Action Group (TDAG). (2012). *Trees in the Townscape. A Aguide for Decision Makers*. https://www.tdag.org.uk/trees-in-the-townscape.html

Weinstein, B. G., Marconi, S., Aubry-Kientz, M., Vincent, G., Senyondo, H., & White, E. P. (2020). DeepForest: A Python package for RGB deep learning tree crown delineation. *Methods in Ecology and Evolution*, *11*(12), 1743–1751. https://doi.org/10.1111/2041-210X.13472

Weinstein, B. G., Marconi, S., Bohlman, S., Zare, A., & White, E. (2019). Individual Tree-Crown Detection in RGB Imagery Using Semi-Supervised Deep Learning Neural Networks. *Remote Sensing 2019, Vol. 11, Page 1309*, *11*(11), 1309. https://doi.org/10.3390/RS11111309

Wu, Q. (2021). Leafmap: A Python package for interactive mapping and geospatial analysis with minimal coding in a Jupyter environment. *Journal of Open Source Software*, *6*(63), 3414. https://doi.org/10.21105/JOSS.03414

Yang, L., Wu, X., Praun, E., & Ma, X. (2009). Tree detection from aerial imagery. *GIS: Proceedings of the ACM International Symposium on Advances in Geographic Information Systems*, 131–137. https://doi.org/10.1145/1653771.1653792

Yang, S., Chong, A., Liu, P., & Biljecki, F. (2025). Thermal comfort in sight: Thermal affordance and its visual assessment for sustainable streetscape design. *Building and Environment*, *271*, 112569. https://doi.org/10.1016/J.BUILDENV.2025.112569

Yuan, Y., Santamouris, M., Xu, D., Geng, X., Li, C., Cheng, W., Su, L., Xiong, P., Fan, Z., Wang, X., & Liao, C. (2025). Surface urban heat island effects intensify more rapidly in lower income countries. *Npj Urban Sustainability*, *5*(1), 1–11. https://doi.org/10.1038/S42949-025-00198-9;SUBJMETA

Zhu, S., Yang, Y., Yan, Y., Causone, F., Jin, X., Zhou, X., & Shi, X. (2022). An evidence-based framework for designing urban green infrastructure morphology to reduce urban building energy use in a hot-humid climate. *Building and Environment*, *219*, 109181. https://doi.org/10.1016/J.BUILDENV.2022.109181